Investigation of the global translational response to oxidative stress in the model archaeon *Haloferax volcanii* reveals untranslated small RNAs with ribosome occupancy

Emma Dallon[a], Haley M. Moran[b], Sadhana R. Chidambaran[a], Arman Kian[a], Betty Y.H. Huang[a], Stephen D. Fried[b,c], Jocelyne DiRuggiero[a,d*]

[a] Department of Biology, Johns Hopkins University, Baltimore, Maryland, USA

[b] Department of Chemistry, Johns Hopkins University, Baltimore, Maryland, USA

[c] T. C. Jenkins Department of Biophysics, Johns Hopkins University, Baltimore, Maryland, USA

[d] Department of Earth and Planetary Sciences, Johns Hopkins University, Baltimore, Maryland, USA

***Corresponding author:** Jocelyne DiRuggiero

Email: jdiruggiero@jhu.edu

Abstract

Oxidative stress induces a wide range of cellular damage, often causing disease and cell death. While many organisms are susceptible to the effects of oxidative stress, haloarchaea have adapted to be highly resistant. Several aspects of the haloarchaeal oxidative stress response have been characterized, however little is known about the impacts of oxidative stress at the translation level. Using the model archaeon *Haloferax volcanii*, we performed RNA-seq and ribosome profiling (Ribo-seq) to characterize the global translation landscape during oxidative stress. We identified 281 genes with differential translation efficiency (TE). Downregulated genes were enriched in ribosomal and translation proteins, in addition to peroxidases and genes involved in the TCA cycle. We also observed upregulated TE for several transporters and membrane-bound proteases, highlighting the importance of membrane dynamics during oxidative stress. We additionally identified 42 small noncoding RNAs (sRNAs) with ribosome occupancy. Size distributions of ribosome footprints revealed distinct patterns for coding and noncoding genes, with 12 sRNAs matching the pattern of coding genes, and mass spectrometry confirming the presence of seven small proteins originating from these sRNAs. However, the majority of sRNAs with ribosome occupancy had no evidence of coding potential. Of these ribosome-associated sRNAs, 12 had differential ribosome occupancy or TE during oxidative stress, suggesting that they may play a regulatory role during the oxidative stress response. In combination with the evidence of regulation at the translation level during oxidative stress, this demonstrates the complexity of gene regulation in response to stress.

Importance: Archaea are found in diverse environments, including as members of the human microbiome, and are known to play essential ecological roles in major geochemical cycles. The study of archaeal biology has expanded our understanding of the evolution of eukaryotes, revealed novel biological systems, and increased possible applications for biotechnology and bioremediation. Many archaeal systems, however, have yet to be fully characterized. Using *Haloferax volcanii* as a model, we investigated the global translation landscape during oxidative stress and revealed the presence of several noncoding ribosome-associated sRNAs that likely play a role in translational regulation. This work expands our knowledge of translational regulation in archaea and underscores the complexity of gene regulation during stress response.

Introduction

Since the advent of oxygenic metabolism, oxidative stress has affected most organisms across all domains of life. This stress is associated with reactive oxygen species (ROS) that disrupt cellular redox state and covalently damage essential macromolecules (1-3). While endogenous ROS, including hydrogen peroxide and superoxide, arise as byproducts of oxygen metabolism (1), ROS levels can increase due to environmental stressors (1, 4). Prolonged oxidative stress induces a range of responses, including disease, autophagy, and cell death (5-8). Prokaryotes utilize numerous enzymes that neutralize ROS (9-13), and certain bacteria and archaea, such as haloarchaea, are known to be exceptionally resistant to oxidative stress (4, 14-17).

Archaea have attracted interest because of mounting evidence that they are ancestral to eukaryotes (18). This is reflected in the mosaic nature of archaeal cells with prokaryotic features and yet information processing machinery more closely related to that of eukaryotes (18-20). The study of archaea has led to the discovery of novel biological systems, such as unique lipids and protein modifications not found in other domains (21, 22). These findings shed light on the evolution of eukaryotes from a prokaryotic ancestor (23) and expand possibilities for biotechnology applications (24). However, many archaeal regulatory systems remain poorly characterized, and our knowledge of them lags behind that of bacterial and eukaryotic counterparts. Mechanisms of transcriptional regulation, especially in response to oxidative stress, have been studied in few archaeal species (25-27). A key transcriptional regulator, RosR, was shown to affect the expression of many genes in response to oxidative stress (26). However, while RosR is conserved among haloarchaea, its function varies among species (25). Post-transcriptional regulation by small noncoding RNAs (sRNAs) is critical to stress responses in many prokaryotic organisms (28-31), and has been linked to oxidative stress in several bacteria (32-34) and in the archaeon *H. volcanii* (37). In *H. volcanii*, the most upregulated sRNA during oxidative stress (SHOxi) binds to and destabilizes malic enzyme transcripts, leading to higher cell survival rates during oxidative stress (35). Post-translational regulation has been investigated with eukaryotic-like protein modifications in archaea, such as sampylation (22). Many proteins associated with the oxidative stress response are targeted by sampylation, suggesting it may play a role in its regulation (36).

While many studies have characterized mechanisms of oxidative stress response at the transcriptional, post-transcriptional, and post-translational levels, little is known about the impacts of oxidative stress at the translation level. Translational regulation has been shown to play a major role in various stress conditions in both bacteria and yeast (37-40). In yeast, the global translation landscape during oxidative stress has been explored using ribosome profiling (Ribo-seq), revealing the regulation of several individual genes and general shifts in translation patterns across all genes (41). Mechanisms of translational regulation by proteins and sRNAs during stress have been reported in archaea. The archaeal protein IF6, a homolog to eukaryotic IF6, inhibits translation by binding to the large ribosomal subunit, preventing assembly of the full ribosome, and is overexpressed during thermal stress (42). In *Methanosarcina mazei*, sRNAs were shown to mask the ribosome binding site of target mRNAs to modulate translation in response to nitrogen starvation (43, 44). This mechanism bears resemblance to an oxidative

stress-responsive sRNA in *E. coli* (45). Additionally, proteomic studies in *H. volcanii* have begun to elucidate the differences between transcription and translation during stress responses (46, 47). However a comprehensive study of translational regulation during oxidative stress response has thus far been lacking.

In this work we present evidence of translational regulation during oxidative stress in *H. volcanii*. This model archaeon is well-characterized at the genetic level (48-50) and a range of genetic and biochemical tools are available (51, 52). Recent advances in studying translation in *H. volcanii* (53, 54) have demonstrated that Ribo-seq can be used to detect translational changes, providing a way to probe the effects of oxidative stress on translation. In the present study, we used RNA-seq and Ribo-seq to determine the global translation landscape during oxidative stress response. We identified genes that were regulated at the translation level during oxidative stress and investigated the potential role of ribosome-associated sRNAs in translation regulation during stress response.

Results

We investigated the global translation landscape in *H. volcanii* during oxidative stress by performing RNA-seq and Ribo-seq *on H. volcanii* cultures with and without stress treatment. Ribo-seq, a technique that captures ribosome occupancy across thousands of transcripts, can be used as a proxy for translation (55). By comparing transcription levels from RNA-seq data to ribosome occupancy from Ribo-seq data, we assessed differential expression, ribosome occupancy, and translation efficiency, allowing us to identify genes regulated at the translation level during oxidative stress.

Hundreds of genes, including known oxidative stress-responsive genes, had differential ribosome occupancy during oxidative stress.

Libraries for RNA-seq and Ribo-seq were prepared from four biological replicate cultures treated with 2 mM hydrogen peroxide for one hour to induce oxidative stress, as previously described (35, 56). Four replicates without stress treatment were used as controls. Sequenced reads were aligned to the genome (50) and normalized expression values of transcripts per million (TPM) were calculated (Table S1, Table S2). Using a minimum detection cutoff of 10 TPM per gene, averaged across all biological replicates, we detected 84% of annotated genes in both RNA-seq control and stress samples. For the Ribo-seq data, we detected 74% of annotated genes in control samples and 80% in stress samples.

We calculated differential expression between controls and oxidative stress treatments for the RNA-seq and Ribo-seq datasets (Table S3). Genes with an adjusted p-value <0.05 and an absolute $\log_2$ fold change >1 were considered differentially expressed during oxidative stress. Lowly expressed genes with TPM <10 in both conditions were excluded from the analysis. We found 559 genes with differential RNA expression during oxidative stress, in contrast to 966 genes with differential ribosome occupancy (Fig. 1A, B). We next investigated the differential expression of five previously known oxidative stress-responsive genes. These genes included superoxide dismutase, catalase, a universal stress protein (HVO_RS06755), and a ssDNA binding

131 replication protein (HVO_RS06110); the latter two were both reported as upregulated proteins
132 in *H. volcanii* under hypochlorite stress (47). All showed significant upregulation in both RNA-
133 seq and Ribo-seq datasets (Fig1A, B; Table S4), implying our experimental approach
134 recapitulates known aspects of oxidative stress response. We also observed upregulation of a
135 gene involved in metal homeostasis (HVO_RS07285; Fig1A, B; Table S4) and downregulation of
136 four others (HVO_RS00195-210; HVO_RS07290; Fig1A, B; Table S4), consistent with previous
137 findings (47).
138
139 We then tested the hypothesis that genes with differential transcript expression would have
140 differential ribosome occupancy, as transcripts highly abundant during oxidative stress would
141 likely be bound by a higher number of ribosomes than transcripts with low abundance. By
142 comparing significant gene lists from RNA-seq and Ribo-seq data, we identified 320 genes with
143 both differential RNA expression and ribosome occupancy during stress. The remaining 646
144 genes changed only in ribosome occupancy during stress (67% of all genes with differential
145 ribosome occupancy; Fig. S1). Several genes had differential ribosome occupancy in accordance
146 with previously published proteomics data (HVO_RS02870-*msrA;* HVO_RS04695-cysteine
147 desulfurase; Table S3; (47)). Overall, in both RNA-seq and Ribo-seq datasets, we detected the
148 majority of annotated genes and identified hundreds of genes with differential ribosome
149 occupancy during oxidative stress. Of genes with differential ribosome occupancy, only one
150 third (33%) also had differential transcript expression, while two thirds (67%) only had changes
151 in ribosome occupancy.
152
153 **Translation efficiency revealed global downregulation of translation during oxidative stress.**
154 To increase the stringency of our analysis and identify genes that were regulated uniquely at
155 the translation level, we calculated translation efficiency (TE). This quantity is defined as the
156 ratio between the Ribo-seq fold change and the RNA-seq fold change and was used for
157 differential expression analysis (Table S3). TE values account for changes in transcript
158 availability and identifies genes that change only at the Ribo-seq or RNA-seq level, eliminating
159 those that change proportionally in both. 281 genes were found to have significant differential
160 TE (Fig. 1C; adjusted p-value <0.05, absolute $\log_2$ fold change >1). When comparing genes with
161 differential TE to those with differential transcript expression and differential ribosome
162 occupancy, we found that the majority were indeed changing primarily at the level of
163 translation (Fig. 1D).
164
165 We investigated some basic properties of transcripts with differential TE to determine whether
166 they were distinct from the overall transcriptome. Several characteristics were explored,
167 including gene size, presence of 5' UTR, and amino acid frequency. The average and range of
168 sizes for genes with differential expression and differential ribosome occupancy were similar to
169 that of all mRNAs. Genes with differential TE had a slightly smaller average size, likely due to a
170 narrower size range of significant genes (Table S5). We observed no differences in amino acid
171 or codon frequencies for genes with differential TE (Fig. S2), suggesting the effect is not
172 governed by tRNA levels (57, 58). We also investigated the proportion of leaderless transcripts
173 in genes with differential TE because 72% of transcripts in *H. volcanii* lack a 5' UTR (59). We
174 observed no difference in the proportion of leaderless transcripts compared to the whole

175 transcriptome (Table S5) and found that, like the majority of the *H. volcanii* transcriptome, most
176 genes with differential TE lack a 5' UTR.
177
178 We then investigated whether there were functional enrichments in genes with differential TE
179 during oxidative stress. We performed a gene ontology analysis using PANTHER generic
180 mapping (60, 61), with enrichment determined using Fisher's test and FDR correction, and
181 KEGG pathway enrichment analysis using the STRING database (62), both of which rely on
182 homology-based predictions. Approximately half of all annotated genes for *H. volcanii* were
183 assigned to functional categories using PANTHER (Fig. 1E), yet very few significant functional
184 enrichments were found among genes with differential TE. Among genes with downregulated
185 TE during oxidative stress, we found enrichment of genes related to translation, with ribosomal
186 proteins and translation proteins having GO fold enrichments of 4.41 (FDR = 0.0005) and 3.39
187 (FDR = 0.0008), respectively, detected by GO enrichment tests. Enrichment of ribosomal
188 proteins was also found by KEGG analysis (FDR = 0.00093). We observed differential TE for
189 many genes related to redox homeostasis. Among downregulated genes, this included an
190 enrichment of peroxidases (GO; fold enrichment = 9.5, FDR = 0.0213) and genes involved in the
191 TCA cycle (KEGG; FDR = 0.0242). When analyzing genes with upregulated TE during oxidative
192 stress we found no statistical overrepresentation of any functional categories. The most
193 upregulated TE (HVO_RS20570; TE fold change of 2.79; Table S6) was for small protein of 51
194 amino acids classified by NCBI as a rubrerythrin-like domain-containing protein. We also
195 observed some interesting trends with functional categories, including an increase, albeit not
196 statistically significant, in transporters and protein modifying enzymes (Fig. 1E). Of particular
197 interest were two genes that encode membrane-bound proteases Sec11a (HVO_RS17270;
198 Table S6) and RhoI (HVO_RS11815; Table S6). Sec11a is one of two known Type I signal
199 peptidases in *H. volcanii*. Direct substrates for each are unknown (63, 64) and, in contrast to
200 Sec11a, the expression and translation of its counterpart (HVO_RS04715) was unaffected by
201 stress conditions. RhoI is one of two known rhomboid proteases in *H. volcanii.* While its
202 substrates are unknown, rhomboid proteases are well-conserved across domains and have
203 been found to play roles in a wide variety of cellular processes (65, 66), including glycosylation
204 of the S-layer in *H. volcanii* (67, 68). The increased translation of these genes may indicate the
205 importance of membrane dynamics during oxidative stress response.
206
207 In addition to investigating functional categories of genes with differential TE, we sought to
208 identify whether specific pathways were susceptible to translational regulation during oxidative
209 stress. To do so, we used the STRING database to predict interactions between genes with
210 upregulated or downregulated TE. We observed few predicted interactions among upregulated
211 genes (Fig. S3). In contrast, genes with downregulated TE formed a larger network containing
212 many functional clusters (Fig. 1F). The two largest clusters consisted of ribosome related genes,
213 including many ribosomal proteins, and genes related to the TCA cycle. The next largest
214 clusters, with 4 genes each, were classified as related to oxidative phosphorylation, pyrimidine
215 biosynthesis, and putative translation initiation factors. These interaction networks suggest
216 that, while translation is generally downregulated, specific pathways undergo targeted
217 translational regulation to modulate metabolic activity within cells.
218

While the majority of genes with differential TE were regulated only at the translational level, we observed that 5% of genes with differential TE were regulated (absolute $\log_2$ fold change >1) at both the transcriptional and translational levels. HVO_RS04895, upregulated for ribosome occupancy and TE (Table S6), encodes a protein with a transmembrane domain, and is known to be upregulated at the transcriptional level during oxidative stress by transcriptional regulator OxsR (69). We additionally observed two genes with a unique regulation pattern of downregulated TE and upregulation of both RNA expression and ribosome occupancy (Table S6). These two genes encode KatG (HVO_RS13250), a catalase/peroxidase that uses hydrogen peroxide as its substrate (70, 71), and DpsA (HVO_RS07285), a DNA starvation/stationary phase protection protein (72, 73). Previously published proteomics data showed no change in protein levels for KatG, and upregulation for DpsA (47). The regulation patterns we observed with Ribo-seq suggested that, in some cases, transcriptional regulation may give an incomplete picture of protein expression during oxidative stress, and translational regulation may act as an additional modulator to quickly titrate protein levels during stress response. In our characterization of genes with differential TE during oxidative stress, we observed no distinct chemical or physical properties to distinguish genes that undergo translational regulation. We found that many ribosome and translation-associated genes have decreased translation, suggesting a global downregulation of translation in response to stress. We also observed differential translation of genes related to redox homeostasis and membrane dynamics, with many transporters and membrane-bound proteases upregulated during oxidative stress. Several genes with differential translation were regulated at both the transcriptional and translational levels, highlighting the likelihood that multiple levels of gene regulation are necessary to modulate protein expression in response to stress.

Many small noncoding RNAs had ribosome occupancy.

As expected, most ribosome footprints in our analysis corresponded to coding genes. However, it was remarkable to find that several small noncoding RNAs (sRNAs), as previously identified using sRNA-seq (56), had ribosome occupancy. In total, we found that 42 out of 56 sRNAs detected in our RNA-seq dataset had ribosome occupancy (TPM >10; Table S7), of which 17 sRNAs exhibited differential ribosome occupancy or differential TE during oxidative stress. We used several computational approaches to determine whether sRNAs with ribosome occupancy encoded putative small proteins (smORFs; Fig. 2A). By searching public databases, we found nine annotated smORFs encoded by sRNAs (Fig. 2A). Of these, three have been detected by mass spectrometry (MS) as reported in the Archaeal Proteome Project database (74). Next, we used REPARATION (75) a program that predicts novel ORFs, including smORFs, from ribosome profiling data (54). We found that 82% of all proteins in the annotated proteome were accurately predicted by REPARATION using our ribosome profiling data (Table S8); this included 436 of 542 (80%) annotated smORFs (less than or equal to 100 amino acids). In addition, REPARATION predicted 194 novel genes (Table S9); only seven of these were small proteins and one was a ribosome-associated sRNA (Fig. 2A). While REPARATION indicated a lack of smORFs encoded by sRNAs, software that predicted ORFs based on sequence alone was overly permissive. ORFfinder (Fig. 2A; (76)) predicted ORFs in sRNAs sequences even when no stop codon was contained within or around the sRNA sequence (Table S10). With conflicting predictions from our computational analyses, and evidence of coding potential for only 10 out

263 of 42 sRNAs with ribosome occupancy (Fig. 2A), we sought to further explore the nature of the
264 ribosome occupancy on sRNAs using ribosome footprint length distribution.
265
266 **Size distributions of ribosome footprints revealed distinct patterns for coding and noncoding**
267 **genes.**
268 Ribosome footprint length distributions of coding genes, noncoding genes, and sRNAs were
269 used to explore the coding potential of ribosome-associated sRNAs. The distribution of
270 footprint lengths for coding genes (both for single genes and the sum of all coding genes)
271 showed that most footprints were between 24 and 27 nucleotides (nt) in length (Fig. 2B). This
272 was supported by previous work reporting that the footprint length for elongating ribosomes
273 was 27 nt (53). In contrast, we found that the distribution for noncoding genes, such as rRNAs,
274 SRP RNA, RNaseP RNA, and tRNAs, had a footprint pattern distinct from that of coding genes
275 (Fig. 2B). We performed clustering analysis on the footprint length distributions of coding and
276 noncoding genes, and sRNAs of interest, using the minimum number of clusters to separate
277 known coding genes from rRNAs and tRNAs. When performing clustering using only sRNAs with
278 annotated smORFs (Fig. S4A), we observed that those with low total read counts (Fig. S4B) did
279 not cluster with coding genes, thus suggesting that a minimum of 65 read counts across all
280 biological replicates was required to distinguish sRNAs with coding potential. Using this
281 threshold value, we found that 12 sRNAs clustered with known coding genes (Fig. 2B), seven of
282 which were sRNAs with annotated smORFs. The high proportion of sRNAs with annotated
283 smORFs included in the coding cluster suggests that this method may distinguish coding genes
284 from known noncoding genes when high enough read counts are available. However, 12 sRNAs
285 with ribosome occupancy remained that had neither an annotated smORF nor a distribution
286 similar to coding genes.
287
288 **Discovery of small proteins encoded by sRNA transcripts.**
289 Using another approach, we performed liquid chromatography tandem mass spectrometry
290 analysis (LC-MS/MS) to validate predictions of coding sRNAs and determine whether small
291 proteins encoded by sRNAs could be detected. In this experiment we used three biological
292 replicates with and without oxidative stress treatment; the stress treatment was essential to
293 ensure expression of stress-responsive sRNAs. To deplete high molecular weight proteins, we
294 sequentially processed the cell lysates through two sizes of centrifugal filters, first a 100 kDa
295 filter and then a 30 kDa filter, (Fig. S5). Our label-free quantitation differential expression
296 analysis detected 2,095 proteins filtered to an FDR of 5% and at least two peptide spectrum
297 matches (PSMs), accounting for 53% of the total proteome of *H. volcanii*. The median protein
298 sequence coverage of 59% was similar to other high-quality MS datasets reported for *H.*
299 *volcanii* (74). Previous studies (77) have demonstrated that centrifugal filtering is an imperfect
300 means to enrich for small proteins, and indeed the sizes of the proteins we detected were
301 roughly representative of the total proteome (Fig. 3A). Moreover, we did not detect any protein
302 smaller than 25 amino acids, even though smORFs are predicted to encode proteins as short as
303 10 amino acids (Fig. 3B). Nevertheless, we detected a total of 235 smORFs (Fig. 3B) ranging
304 from 31-100 amino acids, accounting for 40% of annotated smORFs (Table S11). Seven of these
305 smORFs were encoded in putative sRNAs, including four with prior annotations (Fig. 2A; Table
306 S12), and five out of the seven sRNA-encoded detected proteins had their ribosome footprint

307 length distribution cluster with known coding genes (Fig. 2B). There still remained, however,
308 seven sRNAs with ribosome occupancy in the coding cluster for which we were unable to detect
309 evidence at the protein level.
310
311 To further investigate sRNAs with ribosome occupancy, we selected several of them for
312 western blot analysis. These included one sRNA with read counts below the minimum threshold
313 for clustering (sRNA_38), one sRNA not contained in the coding cluster (sRNA_83), 3 sRNAs
314 contained in the coding cluster that were not detected by MS (sRNA_20, sRNA_61, and SHOxi),
315 and two of the MS-detected smORFs (sRNA_KL, sRNA_93). The selected sRNAs were tagged
316 with a 3xFLAG tag after the putative start codon and cloned into *H. volcanii* on an
317 overexpression plasmid (Fig. 3C; Table S13). 150 bp upstream and 50 bp downstream of the
318 sRNAs were included to capture native promoters. sRNA_20 had multiple putative ORFs, so we
319 tagged two start codons (including one corresponding to a prior annotation). Both MS-detected
320 smORFs (sRNA_KL, sRNA_93) were detected by our western blot analysis, but we did not detect
321 any other tagged sRNAs (Fig. 3D). Despite having both expression level and ribosome occupancy
322 exceeding that of sRNA_KL and sRNA_93 (Table S13), no signal was detected for SHOxi and
323 sRNA_61, indicating they are most likely noncoding. From the analyses above, we detected
324 seven smORFs encoded by sRNAs using LC-MS/MS, including three novel smORFs not previously
325 annotated. However, some sRNAs, such as sRNA_61 and SHOxi, had no coding potential, were
326 not detected by MS or western blotting, but yet demonstrated high ribosome occupancy,
327 exceeding that of many coding regions.
328
329 **Ribosome-associated sRNAs may play regulatory roles during oxidative stress.**
330 We were particularly interested in 17 stress-responsive sRNAs that had differential ribosome
331 occupancy or TE in stress-treated samples (Fig. 4A). Five of these had an annotated smORFs and
332 12 had no evidence of coding potential. We repeated the ribosome footprint length clustering
333 analysis described above for Ribo-seq data from oxidative stress samples. We found that of the
334 12 sRNAs with no evidence of coding potential (unannotated), one did not meet the read count
335 threshold and was removed from the analysis, three clustered with coding genes, and nine did
336 not (Fig. 4B). We hypothesized that these nine stress-responsive sRNAs with high ribosome
337 occupancy may play a regulatory role during oxidative stress and sought to explore their
338 functional roles using a suite of *in silico* methods. We note that SHOxi has been previously
339 characterized (35) and sRNA_41 is annotated as encoding an smORF, thus neither were
340 included in this analysis.
341
342 We first determined whether these sRNAs were conserved by performing a blastn search. Five
343 had homology with one or more halophilic species, two of which had the majority of hits in a
344 region that overlapped with an upstream gene on the opposite strand. The remaining two had
345 no homology with any other species. We selected the three sRNAs (sRNA_58, sRNA_77, and
346 sRNA_83) with homology to at least one other species and that did not overlap with any genes
347 to further investigate their role in *H. volcanii* oxidative stress response. We performed a
348 multiple sequence alignment and predicted the consensus structures for sRNA_58, sRNA_77,
349 and sRNA_83 using LocARNA (78) and all hits from our previous blastn search as input. Each
350 sRNA showed a high potential for secondary structure and high conservation between species

351 (Fig. 5A; Fig. S6). We also predicted putative mRNA targets using IntaRNA (Fig. 5B; Tables S14-
352 16; 79) and determined which of those predicted targets had differential ribosome occupancy
353 or TE during oxidative stress. sRNA_58 had the fewest high confidence ($p < 0.01$) predicted
354 targets, and only five out of 29 (17%) of those predicted targets had differential ribosome
355 occupancy or TE in response to oxidative stress. In contrast, sRNA_77 and sRNA_83 had many
356 targets predicted with high confidence and 14 out of 44 (32%) putative mRNA targets for
357 sRNA_83, and 19 out of 42 (45%) putative mRNA targets for sRNA_77 were differentially
358 translated in response to oxidative stress. Overall, eight sRNAs with differential ribosome
359 occupancy or TE during oxidative stress did not have coding potential, one of which was
360 previously characterized (35). Five were found to be conserved among halophilic species and
361 two had many putative mRNA targets that were differentially regulated at the translation level
362 during oxidative stress.
363
364 **sRNA knockouts have similar phenotype to WT during oxidative stress.**
365 To explore the functional role of ribosome-associated sRNAs during oxidative stress, we
366 generated sRNA knockouts. Three sRNAs with a range of ribosome occupancy were selected.
367 sRNA_24 represented the lowest range (TPM <10), with sRNA_83 and sRNA_20 representing
368 mid-range (50-100 TPM) and high ribosome occupancy (>200 TPM), respectively. Knockouts
369 were generated as previously described (80), followed by whole genome sequencing to verify
370 complete deletion of sRNAs. We did not observe any phenotypic differences from the WT
371 during oxidative stress for our sRNA knockouts, when using H_2O_2 as treatment (Fig. S7A, B).
372
373 In an attempt to identify experimentally putative targets for these sRNAs, we performed RNA-
374 seq with three biological replicates each of WT and the sRNA knockout strains exposed to
375 oxidative stress and WT without stress as a control, as previously described (35). The RNA-seq
376 data were analyzed as described above with significance cutoffs of adjusted p-value <0.05 and
377 absolute $\log_2$ fold change >1. No genes were significantly upregulated or downregulated for
378 sRNA_83 and sRNA_20 knockout strains when compared to the WT strain under oxidative
379 stress (Fig. S7C, D). We found 7 genes significantly upregulated for the sRNA_24 knockout strain
380 when compared to the WT (Fig. S7E). qPCR further validated these results (Fig. S7F). We also
381 found that in the presence of sRNA_24 (WT strain) and oxidative stress treatment, 6 of the
382 genes described above had upregulated expression compared to untreated controls, and one
383 was downregulated for both ribosome occupancy and TE (Table S17). For all 7 significant
384 targets, the fold change increased substantially in the absence of sRNA_24, suggesting that this
385 sRNA may play a role in downregulating expression of these genes. Additionally, we observed
386 that the upregulated 9 genes with p-value < 0.05 in the sRNA_24 knockout strain were located
387 directly downstream of sRNA_24 in the genome of *H. volcanii* (Fig. S7G), and three of these
388 targets were members of an operon involved in glycerol metabolism in *H. volcanii* (Table S18,
389 81).
390

391 # Discussion

392 In this work, we investigated the global translation landscape of the model archaeon *H. volcanii*
393 during oxidative stress. While previous studies in *H. volcanii* have revealed changes in protein
394 levels during oxidative stress using MS (47), this method does not distinguish between

395 transcriptional and translational regulation. It is also known that transcript data from RNA-seq
396 and protein data from MS have modest and highly variable correlation rates (82, 83), leading to
397 questions regarding the processes that govern translation regulation. Using RNA-seq and Ribo-
398 seq, we examined ribosome occupancy and TE to better understand regulation at the level of
399 translation.
400
401 Our analysis revealed that hundreds of genes had differential TE in *H. volcanii* during oxidative
402 stress. We observed global downregulation of translation and ribosomal proteins, suggesting a
403 major slowdown of *de novo* protein biogenesis during oxidative stress. While previous studies
404 in eukaryotes have found arrest of translation during stress (41, 84, 85), including sequestration
405 of translationally inactive complexes within stress granules (86, 87), archaeal studies diverge. In
406 *H. volcanii,* downregulation of ribosomal proteins has been shown at the level of transcription
407 (56), while MS data showed upregulation of translation proteins, including ribosomal proteins,
408 during oxidative stress (47). However, our interaction networks analysis using the STRING
409 database further supported the downregulation of translation and ribosomal genes, with many
410 ribosomal proteins included in the largest cluster, suggesting that in addition to transcriptional
411 regulation, numerous genes were also regulated at the translation level. Among genes with
412 upregulated translation during oxidative stress, we found many transporters, in accordance
413 with data previously acquired from MS (47). In contrast, at the transcriptional level,
414 transporters have been shown to be an enriched category in downregulated genes during
415 oxidative stress (56). The differences found in RNA-seq, Ribo-seq, and MS data imply that
416 multiple levels of regulation might be used to modulate protein expression during stress
417 response. Complex gene regulation has been characterized in both eukaryotes and bacteria,
418 including examples such as combined transcription and translation regulation of a cold shock
419 protein in mammals (88), quorum sensing signals in *Agrobacterium tumefaciens* (89, 90), and
420 attenuation of the tryptophan operon in *E. coli* (91, 92). Indeed, the interplay of transcriptional
421 and translational regulation to modulate protein expression might enable a fast response to
422 changing environmental conditions.
423
424 Remarkably, we found that many sRNAs previously determined to be noncoding (56) had high
425 ribosome occupancy, suggesting that association with ribosomes was not limited to active
426 translation. We found that among these sRNAs, some encoded annotated smORFs, some had
427 footprint distributions matching that of coding genes, and we detected seven small proteins
428 encoded by sRNAs using MS. It is important to note, however, that encoding small proteins
429 does not preclude these sRNAs from playing regulatory roles post-transcriptionally. In bacteria,
430 the presence of dual function sRNAs that encode proteins in addition to performing regulatory
431 functions has been well established (93-95). Archaea have also been proposed to utilize dual
432 function sRNAs, particularly under nitrogen starvation (96). This suggests that, as in other
433 organisms (93, 97), *H. volcanii* may utilize dual function sRNAs during oxidative stress response.
434
435 Many sRNAs had no evidence of coding potential, even when individually tagged and probed,
436 while smORFs detected by LC-MS were also detected by tagging and western blot. Several of
437 the sRNAs for which no proteins were detected had higher ribosome occupancy than sRNAs
438 with smORFs detected by MS and western blotting. While Ribo-seq is potentially the most

439 sensitive method for detecting smORFs (54, 96), there is enduring concern it may over-
440 represent the number of sRNAs being translated (98, 99), as we have observed here, making
441 MS proteomics an important filter to provide direct protein-level evidence. We additionally
442 utilized the distributions of ribosome footprint lengths to investigate coding potential of sRNAs
443 with ribosome occupancy. Using this analysis, we observed that the majority of coding genes
444 and sRNAs with annotated smORFs clustered together. We were further able to separate the
445 majority of known noncoding genes from known coding genes, thus suggesting that this
446 method can be used to provide an additional layer of information to increase confidence that
447 an sRNA has coding potential. However, this method requires a minimal read counts to
448 discriminate coding and noncoding genes. Similarly, it is possible that low abundance may limit
449 detection of small proteins by MS or western blotting. For lowly expressed sRNAs,
450 overexpression with an inducible promoter may be required for detection, as was found
451 previously (54). For sRNAs with higher expression, however, the lack of protein detection
452 despite high ribosome occupancy implies other mechanisms for the association of these sRNAs
453 with the ribosome.
454
455 Our data suggest that these sRNAs with no evidence of coding potential are closely associated
456 to ribosomes and may interact directly with ribosomes. While it is known that RNAs with
457 secondary structure are resistant to digestion, the inherently small size of these sRNAs would
458 preclude them from separating with monosomes in a sucrose gradient, thus suggesting that
459 they are specifically associated either with ribosomes or mRNAs bound to ribosomes. Prior
460 studies have reported the presence of sRNAs associated with ribosomes in *H. volcanii*,
461 particularly under stress conditions (100, 101). Sequencing and northern blotting of sRNAs that
462 co-purify with ribosomes identified a tRNA-derived fragment that bound the ribosome small
463 subunit, inhibiting peptide bond formation (100), and an intergenic sRNA that interacted with
464 the large subunit and targeted the translation of a specific mRNA (101).
465
466 The deletion of three ribosome-associated sRNA did not result in a growth phenotype during
467 oxidative stress and showed little to no change in the expression level of other genes. This
468 suggests that these sRNAs may not directly modulate transcript stability as some sRNAs in both
469 bacteria (32, 102, 103) and archaea (104, 105). In *H. volcanii*, for example, SHOxi destabilized its
470 mRNA target by complementary base pairing (35). Alternatively, the deletions of single sRNAs
471 may be insufficient to observe the effects of these sRNAs, as has been observed in bacteria
472 (106, 107). Knocking out multiple stress-responsive ribosome-associated sRNAs could further
473 elucidate their role during oxidative stress. Taken together, the data suggest that several
474 stress-associated sRNAs in *H. volcanii* are closely associated with ribosomes but are not directly
475 impacting mRNA stability.
476
477 Using RNA-seq and Ribo-seq in a model archaeon, we demonstrated global and targeted
478 regulation at the translation level during oxidative stress. We additionally revealed the
479 presence of several untranslated ribosome-associated sRNAs in *H. volcanii* that likely play a role
480 in translational regulation during oxidative stress. While the mechanisms of action of these
481 sRNA remain to be fully explored, this study highlights the use of multiple levels of gene

482 regulation to modulate protein expression in response to stress and provides the groundwork
483 to understand the complexities of oxidative stress response at the translation level.
484

485 Materials and Methods

486 Cell culturing and oxidative stress treatment

487 *Haloferax volcanii* DS2 strain H98 (80) was grown in liquid Hv-YPC (80) supplemented with 40
488 mg/mL thymidine at 42°C, with shaking, to OD >0.5. Cultures were diluted into fresh media to
489 an OD of 0.01 and grown to OD 0.4-0.6. For oxidative stress treatment, cultures were incubated
490 with 2mM H_2O_2 for one hour at 42°C with shaking, as previously described (56).
491

492 Ribosome profiling

493 Ribo-seq was performed as previously described (53, 108). In brief, cultures were flash frozen in
494 liquid nitrogen and lysed by cryogenic mill, using 55 g of frozen culture and 100 µg/mL of
495 anisomycin. Ribosomes were collected by ultracentrifugation on a 1 M sucrose cushion using a
496 Ti45 rotor at 185,511x*g* (40,000 rpm) for three hours at 4°C. Polysomes were digested using
497 MNase and separated using a 10-50% sucrose gradient (Fig. S8A). RNA from monosome
498 fractions was isolated with Trizol LS reagent, followed by size selection (Fig. S8B), and
499 generation of libraries for high-throughput sequencing (Fig. S8C, D). Libraries were sequenced
500 by Novogene (150 bp, paired-end reads, NovaSeq).
501

502 RNA-seq

503 RNA-seq libraries were prepared using 20 mL of culture pelleted by centrifugation. RNA
504 extraction was performed as previously described (56) using a Quick-RNA Miniprep kit (Zymo).
505 rRNA was depleted using 2.5 µg of DNase-treated RNA and the Ribo-Zero rRNA removal kit for
506 bacteria (Illumina). The SMARTer Stranded RNA-Seq kit (Takara Bio) was used to prepare the
507 libraries with 100 ng RNA, dual-index primers, and 12 PCR cycles. Libraries were sequenced by
508 Novogene (150 bp, paired-end reads, NovaSeq). For knockout strains, RNA was prepared as
509 described above, using 3 replicates per strain. All strains were treated with H_2O_2, with 3
510 replicates of untreated WT as controls. Library preparation and sequencing were performed by
511 SeqCenter in Pittsburgh, PA (150 bp, paired-end reads, NovaSeq X plus) using Illumina's
512 Stranded Total RNA Prep Ligation with Ribo-Zero Plus kit and custom probes.
513

514 Analysis of sequencing data

515 Demultiplexed reads provided by Novogene and SeqCenter were analyzed using only forward
516 reads for Ribo-seq libraries and both reads for RNA-seq libraries. For full analysis details, see
517 Table S19. Adapters were trimmed using Trim Galore (109,
518 https://github.com/FelixKrueger/TrimGalore) and reads were aligned to rRNA genes using
519 Bowtie (110). Unaligned reads (those not aligning to rRNA) were written to a new file and used
520 for genome alignment, which was performed using Bowtie and the *H. volcanii* DS2 genome
521 assembly ASM2568v1 from NCBI (50). Samtools (111) was used to generate bam and sorted
522 bam files. Coverage and depth were calculated using samtools and bedtools. Average depth per
523 chromosome was calculated using a custom Python script. TPM were calculated using StringTie
524 (112), with a provided reference annotation file (gff from NCBI Refseq assembly

525 GCF_000025685.1 downloaded March 2023 with added entries for sRNAs). Read counts were
526 calculated using featureCounts (113). See Tables S20, S21, and S22 for statistical summaries of
527 all analyses.
528
529 **Differential expression and TE analysis**
530 Differential expression was determined using DESeq2 (114). For RNA-seq and Ribo-seq data, the
531 variable of interest was experimental condition. For TE, the ratio between Ribo-seq and RNA-
532 seq was used, in addition to two variables of interest: sample (RNA-seq or Ribo-seq) and
533 experimental condition. For full details, see Table S19.
534
535 **Characterization of significant genes**
536 The number of leaderless genes was determined using published data that characterized 1851
537 annotated genes as leadered or leaderless (59). 68% of genes with differential TE were
538 uncharacterized and therefore not considered in calculations for the percent of leaderless
539 genes. Custom Python scripts were used to calculate percent of leaderless genes, codon
540 frequencies, and amino acid frequencies. Heatmaps were generated using R. The STRING
541 database (web version 12.0; 62) was used to determine KEGG enrichments with default settings
542 and MCL clustering. 84% of genes with differential TE were successfully mapped to the STRING
543 database. The PANTHER database (web version 19.0) was used to generate a generic mapping
544 file (61, 115) for the *H. volcanii* DS2 protein fasta file downloaded from NCBI.
545 Overrepresentation tests were conducted using Fisher's test and FDR correction.
546
547 **smORF prediction**
548 For ORF prediction using the web version of Open Reading Frame Finder (ORFfinder, NCBI; 76),
549 a minimal length of 30nt and alternative initiation codons were allowed. For ORF prediction
550 using Ribo-seq data, an adapted version of REPARATION (75), using blast instead of USEARCH
551 (https://github.com/RickGelhausen/REPARATION_blast) was used. For option details, see Table
552 S18. A custom python script compared and combined predictions with and without Shine-
553 Dalgarno. Predicted genes were visualized using IGV, and a manual scan was conducted to
554 compare overlap between replicates for control or oxidative stress treatment. Predicted genes
555 were required to be present in at least 3 biological replicates. Novel gene lists for control and
556 stress samples were then combined.
557
558 **Footprint distribution clustering**
559 Lengths of reads aligning to individual genes were obtained using a custom Bash script,
560 followed by analysis using R to generate heatmaps. Clustering was performed using the
561 pheatmap (https://github.com/raivokolde/pheatmap) package with default settings and the
562 minimum number of clusters required to separate rRNA from known coding genes in control
563 samples.
564
565 **Mass spectrometry sample preparation**
566 Samples for mass spectrometry were prepared using 600 mL cultures from three replicates; half
567 of the culture was used for control samples and the other half was treated with H_2O_2. Cells
568 were pelleted by centrifugation then resuspended in 8 mL lysis buffer (2 M NaCl, 8 M urea, 0.1

569 M Tris-Cl, 10 mM DTT) and flash frozen. Resuspension was ground in a cryogenic mill (SPEX
570 6870) with a 1 minute pre-cool, then 8 cycles of alternating 1 minute of run time and 1 minute
571 of cool time, at a rate of 8 cycles/second. The thawed lysate was spun twice at 15000 x*g* for 15
572 minutes at 4°C. Lysis buffer was added to a volume of 10 mL, then filtered through a 0.2-micron
573 syringe filter and brought to a final volume of 12 mL with lysis buffer. Size selection was
574 performed by centrifugation in 100K MWCO filters (Pall) at 5000 x*g* for 2 hours at room
575 temperature, then centrifugation in 30K MWCO filters (Pall) at 5000 x*g* for 45 minutes at room
576 temperature. Iodoacetamide was added to a final concentration of 54 mM and incubated for 45
577 minutes in the dark at room temperature, followed by addition of 11.1% of volume of
578 trichloroacetic acid. Samples were flash frozen, then incubated at 4°C overnight. Samples were
579 centrifuged at 20000 x*g* for 30 minutes at 4°C and supernatant was removed. Pellets were
580 washed twice with acetone, air-dried for 10 minutes, then resuspended in 50 µL of 8 M urea in
581 phosphate-buffered saline (PBS), pH 7.4 and quantified using the Qubit Protein Assay kit. 30 µg
582 of total protein in 200 µL of 2 M urea in PBS, pH 7.4 were digested with trypsin and prepared
583 for MS as previously described (116).
584
585 **Mass spectrometry acquisition**
586 Chromatographic separation of protein digests was carried out as previously described (117),
587 injecting 1 µg of protein per sample.
588
589 **Mass spectrometry data analysis**
590 The Proteome Discoverer (PD) Software Suite v2.4, Minora Algorithm (ThermoFisher) was used
591 to process mass spectra and perform Label Free Quantification (LFQ), comparing control and
592 stress samples with default settings for all analysis nodes except where specified. Data were
593 searched against the *H. volcanii* DS2 proteome fasta file from Uniprot (entry UP000008243,
594 organism ID 309800; downloaded January 2023). The reference fasta file was appended with
595 additional sequences for putative smORFs. For peptide identification, the Proteome Discoverer
596 Sequest HT node was selected for a tryptic search allowing up to 2 missed cleavages. A
597 precursor mass tolerance of 10 ppm was used for the MS1 level, and a fragment ion tolerance
598 of 0.02 was set at the MS2 level. Methionine oxidation and N-terminus acetylation were
599 allowed as dynamic modifications, with carbamidomethylation on cysteines defined as a static
600 modification. Protein abundance ratio data were exported using a three-level hierarchy
601 (protein > peptide group > consensus features). A minimum of 2 PSMs and maximum FDR of 5%
602 were required to determine detection of novel small proteins. See Table S23 for statistical
603 summaries.
604
605 **Generating tagged sRNAs**
606 sRNA regions (including at minimum 150 bp upstream and 50 bp downstream) were amplified
607 from genomic DNA and cloned into pTA1300 using *Kas*I and *Bam*HI. Ligation products were
608 transformed into DH5α competent cells (NEB), followed by plasmid extraction (QIAprep spin
609 miniprep kit) and verification by Sanger sequencing (GENEWIZ, Azenta). A 3xFLAG tag was
610 added after the predicted start codon using Q5 site-directed mutagenesis (NEB). Purified
611 plasmids were transformed into *H. volcanii* as previously described (118), using the lab strain
612 H98.

613
614 **Western blots**
615 25 mL of culture were pelleted by centrifugation at 10,000 x*g* for 6 minutes at 4°C. Pellets were
616 resuspended in 1 mL lysis buffer (50 mM Tris-HCl pH 7.5, 2 M urea, 0.2% SDS, 0.1 mg/mL EDTA-
617 free protease inhibitor cocktail (Roche)) and lysed with sterile glass beads (119). Protein
618 concentration was quantified using the Qubit Protein Assay kit. Proteins (10-100 µg total) were
619 separated on a 4-15% stain free acrylamide gel (BioRad), transferred to a nitrocellulose
620 membrane, and incubated with anti-Flag monoclonal antibodies conjugated with alkaline
621 phosphatase (1:10,000 dilution; Sigma cat no. A9469), as previously described (119). The
622 antibody:protein complexes were visualized using 0.25 mM CDP-Star Substrate (Tropix) with 1x
623 Nitro-Block-II Enhancer (Invitrogen) and the BioRad ChemiDoc Imager.
624
625 **sRNA in silico tools**
626 Web versions of nucleotide BLAST (120), IntaRNA (79, 121), and LocARNA (78) were used with
627 default settings.
628
629 **Generating knockouts**
630 Knockout strains were generated using the established protocol for *H. volcanii* (80). For
631 sRNA_83, a knockout plasmid was constructed by amplifying upstream and downstream
632 flanking regions from genomic DNA and cloning into pTA131 using *Hind*III, *Xba*I, and *Eco*RI.
633 Knockout plasmids for sRNA_20 and sRNA_24 were generated by Azenta, with upstream and
634 downstream flanking regions cloned into pTA131 using *Hind*III and *Xba*I. Knockout plasmids
635 were transformed into *H. volcanii* (118), strain H98, followed by selection for pop-in (uracil
636 selection) and pop-out (5-FOA selection). Whole genome sequencing of successful pop-outs
637 was performed by Plasmidsaurus using Oxford Nanopore Technology with custom analysis. For
638 ΔsRNA_83 and ΔsRNA_24, no additional mutations were identified. For ΔsRNA_20, two
639 additional point mutations were detected (C->G at position 50,650 in HVO_RS02135; A->G at
640 position 1,284,523 in HVO_RS11505).
641
642 **Knockout phenotyping**
643 To assess survival during acute oxidative stress, 3 replicates of WT and mutant strains were
644 grown as described above in a total volume of 20 mL. 50 µL of culture were plated, and
645 remaining culture was treated with H_2O_2. Cultures were plated on YPC with thymidine and
646 incubated at 42°C for 4 days. Colonies were counted and used to calculate CFUs/mL and
647 percent survival. To assess survival during chronic oxidative stress, 3 replicates of WT and
648 mutant strains were grown as described above. Cultures were diluted into fresh media to an OD
649 of 0.02 and treated with various H_2O_2 concentrations. Cultures were transferred to 100-well
650 plates (250 µL/well) and grown in a Bioscreen C Pro for 42 hours at 42°C with shaking (normal
651 speed, max amplitude, orbital). Absorbance measurements were taken every six hours. Data
652 were plotted using R.
653
654 **qPCR**
655 Samples for qPCR were prepared using 40 mL cultures from 3 replicates; half used for control
656 samples and half treated with H_2O_2. Cells were harvested and RNA was extracted as described

for RNA-seq library preparation. Conversion to cDNA was performed using a Superscript RT III kit (Invitrogen) with random hexamers. qPCR was conducted in 48-well plates with PowerUp™ SYBR™ Green Master Mix (Applied Biosystems, A25742) using the StepOne™ Real-Time PCR System with standard conditions and annealing temperature of 60°C (for primers, see Table S24). Fold change was determined by the Livak method (122).

Data availability

RNA-seq reads, ribosome profiling reads, and annotation files are available on NCBI GEO: GSE293312 (RNA-seq) and GSE293326 (Ribo-seq). The mass spectrometry proteomics data have been deposited to the ProteomeXchange Consortium via the PRIDE (123) partner repository with the dataset identifier PXD062323 and 10.6019/PXD062323. Data analysis scripts are available on GitHub: https://github.com/diruggiero-lab/sRNAs.

Reviewers' access to the manuscript data in public databases:

GEO accession GSE293312 (RNA-seq):

Go to
https://nam02.safelinks.protection.outlook.com/?url=https%3A%2F%2Fwww.ncbi.nlm.nih.gov%2Fgeo%2Fquery%2Facc.cgi%3Facc%3DGSE293312&data=05%7C02%7Cedallon1%40jhu.edu%7Cee49674d5d8f47a9e59808dd73cc9352%7C9fa4f438b1e6473b803f86f8aedf0dec%7C0%7C0%7C638794044694533383%7CUnknown%7CTWFpbGZsb3d8eyJFbXB0eU1hcGkiOnRydWUsIlYiOiIwLjAuMDAwMCIsIlAiOiJXaW4zMiIsIkFOIjoiTWFpbCIsIldUIjoyfQ%3D%3D%7C0%7C%7C%7C&sdata=z5drfRsNagEzuUwOn5VO4lA4u7xSmRBSkTH%2FvQkET2c%3D&reserved=0
Enter token ifkpmmmqnnahhgp into the box

GEO accession GSE293326 (Ribo-seq):

Go to
https://nam02.safelinks.protection.outlook.com/?url=https%3A%2F%2Fwww.ncbi.nlm.nih.gov%2Fgeo%2Fquery%2Facc.cgi%3Facc%3DGSE293326&data=05%7C02%7Cedallon1%40jhu.edu%7C33dc7dc2fad44c80538d08dd73cc9e3f%7C9fa4f438b1e6473b803f86f8aedf0dec%7C0%7C0%7C638794044873836946%7CUnknown%7CTWFpbGZsb3d8eyJFbXB0eU1hcGkiOnRydWUsIlYiOiIwLjAuMDAwMCIsIlAiOiJXaW4zMiIsIkFOIjoiTWFpbCIsIldUIjoyfQ%3D%3D%7C0%7C%7C%7C&sdata=poISC7k8i%2BV%2BMF%2BtNC7hmLGmmisA3Yz%2B8hQQ6PaY6vI%3D&reserved=0
Enter token ibyxikeqppehpgh into the box

Pride accession PXD062323 (MS data)

Log in to the PRIDE website at https://www.ebi.ac.uk/pride/login using the following account details (use Login with your registered email address OR reviewer username (ex: reviewerXXX@ebi.ac.uk):

Username: reviewer_pxd062323@ebi.ac.uk
Password: 0vtHi3HDave2
Project accession: PXD062323
Project DOI: 10.6019/PXD062323

Acknowledgements

This work was supported by US National Science Foundation grants MCB-2034271 and MCB-57951 to JDR and Grant MCB-2045844 to SFD, and by an NIH/NIGMS grant GM140926 to SDF. SDF further acknowledges support from the Camille & Henry Dreyfus Foundation and the Sloan Foundation. HMM is thankful for the Chemistry-Biology Interface Program training grant (NIH-T32GM080189-13) and ED for the Cell, Molecular, Developmental Biology and Biophysics (CMDB) training grant (NIH-T32GM). We thank Dr. Cesar Perez-Fernandez, Dr. Diego Gelsinger, and Frank Liu for experimental advice and helpful discussions. We thank Matthew F. Isada for extensive manuscript editing and helpful discussions.

E.D.: Conceptualization, Methodology, Investigation – RNA-seq, Ribo-seq, mass spectrometry sample preparation, western blots, knockout phenotyping, Formal analysis – analysis of sequencing data, footprint distribution analysis, Visualization, Writing – original draft, Writing – review & editing; H.M.M: Investigation – mass spectrometry sample preparation, mass spectrometry data acquisition, Formal analysis – mass spectrometry data analysis, Writing – review & editing; S.R.C: Formal analysis – DESeq2 analysis for all datasets; A.K.: Investigation – construction of tagged sRNA constructs and sRNA knockout strains, qPCR analysis; B.Y.H.H.: Investigation – construction of tagged sRNA constructs; S.D.F.: Methodology, Writing – review & editing; J.D.: Conceptualization, Methodology, Data analyses, Funding acquisition, Writing – review & editing, Supervision. All authors read and approved the final manuscript.

References

1. Cabiscol Catalā E, Tamarit Sumalla, J, Ros Salvador, J. 2000. Oxidative stress in bacteria and protein damage by reactive oxygen species. Int Microbiol 3:3-8.

2. Seixas AF, Quendera, AP, Sousa, JP, Silva, AFQ, Arraiano, CM, Andrade, JM. 2022. Bacterial response to oxidative stress and RNA oxidation. Front Genet 12:821535.

3. Ezraty B, Gennaris, A, Barras, F, Collet, J. 2017. Oxidative stress, protein damage and repair in bacteria. Nat Rev Microbiol 15:385–396.

4. Maezato Y, Blum, P. 2012. Survival of the fittest: Overcoming oxidative stress at the extremes of acid, heat and metal. Life 2:242.

5. Farrugia G, Balzan, R. 2012. Oxidative stress and programmed cell death in yeast. Front Oncol 2:64.

6. Jelic MD, Mandic, AD, Maricic, SM, Srdjenovic, BU. 2021. Oxidative stress and its role in cancer. J Cancer Res Ther 17:22–28.

7. Teleanu DM, Niculescu, A, Lungu, II, Radu, CI, Vladâcenco, O, Roza, E, Costăchescu, B, Grumezescu, AM, Teleanu, RI. 2022. An overview of oxidative stress, neuroinflammation, and neurodegenerative diseases. Int J Mol Sci 23:5938.

8. Steven S, Frenis, K, Oelze, M, Kalinovic, S, Kuntic, M, Bayo Jimenez, MT, Vujacic-Mirski, K, Helmstädter, J, Kröller-Schön, S, Münzel, T, Daiber, A. 2019. Vascular inflammation and

740 oxidative stress: Major triggers for cardiovascular disease. Oxid Med Cell Longev
741 2019:7092151.

742 9. Johnson LA, Hug, LA. 2019. Distribution of reactive oxygen species defense mechanisms
743 across domain bacteria. Free Radic Biol Med 140:93–102.

744 10. Sato Y, Kameya, M, Fushinobu, S, Wakagi, T, Arai, H, Ishii, M, Igarashi, Y. 2012. A novel
745 enzymatic system against oxidative stress in the thermophilic hydrogen-oxidizing bacterium
746 *Hydrogenobacter thermophilus*. Plos One 7:e34825.

747 11. Cannio R, D'angelo, A, Rossi, M, Bartolucci, S. 2000. A superoxide dismutase from the
748 archaeon *Sulfolobus solfataricus* is an extracellular enzyme and prevents the deactivation by
749 superoxide of cell-bound proteins. Eur J Biochem 267:235–243.

750 12. Takao M, Oikawa, A, Yasui, A. 1990. Characterization of a superoxide dismutase gene from
751 the archaebacterium *Methanobacterium thermoautotrophicum*. Arch Biochem Biophys
752 283:210–216.

753 13. Jeon S, Ishikawa, K. 2002. Identification and characterization of thioredoxin and thioredoxin
754 reductase from *Aeropyrum pernix* K1. Eur J Biochem 269:5423–5430.

755 14. Dea S, Miroslav, R. 2011. Oxidative stress resistance in *Deinococcus radiodurans*. Microbiol
756 Mol Biol Rev 75:133–191.

757 15. Matarredona L, Camacho, M, Zafrilla, B, Bravo-Barrales, G, Esclapez, J, Bonete, M. 2021. The
758 survival of *Haloferax mediterranei* under stressful conditions. Microorganisms 9:336.

759 16. Robinson CK, Webb, K, Kaur, A, Jaruga, P, Dizdaroglu, M, Baliga, NS, Place, A, DiRuggiero, J.
760 2011. A major role for nonenzymatic antioxidant processes in the radioresistance of
761 *Halobacterium salinarum*. J Bacteriol 193:1653–1662.

762 17. Webb KM, Yu, J, Robinson, CK, Noboru, T, Lee, YC, DiRuggiero, J. 2013. Effects of
763 intracellular Mn on the radiation resistance of the halophilic archaeon *Halobacterium*
764 *salinarum*. Extremophiles 17:485–497.

765 18. Eme L, Spang, A, Lombard, J, Stairs, CW, Ettema, TJG. 2017. Archaea and the origin of
766 eukaryotes. Nat Rev Microbio 15:711–723.

767 19. Phung DK, Etienne, C, Batista, M, Langendijk-Genevaux, P, Moalic, Y, Laurent, S, Liuu, S,
768 Morales, V, Jebbar, M, Fichant, G, Bouvier, M, Flament, D, Clouet-d'Orval, B. 2020. RNA
769 processing machineries in archaea: The 5'-3' exoribonuclease aRNase J of the β-CASP family is
770 engaged specifically with the helicase ASH-Ski2 and the 3'-5' exoribonucleolytic RNA exosome
771 machinery. Nucleic Acids Res 48:3832–3847.

772 20. Brochier-Armanet C, Forterre, P, Gribaldo, S. 2011. Phylogeny and evolution of the archaea:
773 One hundred genomes later. Curr Opin Microbiol 14:274–281.

774 21. Řezanka T, Kyselová, L, Murphy, DJ. 2023. Archaeal lipids. Prog Lipid Res 91:101237.

775 22. Humbard MA, Miranda, HV, Lim, J, Krause, DJ, Pritz, JR, Zhou, G, Chen, S, Wells, L, Maupin-
776 Furlow, JA. 2010. Ubiquitin-like small archaeal modifier proteins (SAMPs) in *Haloferax*
777 *volcanii*. Nature 463:54–60.

778 23. Nunoura T, Takaki, Y, Kakuta, J, Nishi, S, Sugahara, J, Kazama, H, Chee, G, Hattori, M, Kanai,
779 A, Atomi, H, Takai, K, Takami, H. 2010. Insights into the evolution of archaea and eukaryotic
780 protein modifier systems revealed by the genome of a novel archaeal group. Nucleic Acids
781 Res 39:3204–3223.

782 24. Haque RU, Paradisi, F, Allers, T. 2020. *Haloferax volcanii* for biotechnology applications:
783 Challenges, current state and perspectives. Appl Microbiol Biotechnol 104:1371–1382.

784 25. Pastor MM, Darnell, CL, Vreugdenhil, A, Schmid, AK. 2024. Rapid rewiring of an archaeal
785 transcription factor function via flexible cis-trans interactions. bioRxiv 2024.11.20.624553.

786 26. Sharma K, Gillum, N, Boyd, JL, Schmid, A. 2012. The RosR transcription factor is required for
787 gene expression dynamics in response to extreme oxidative stress in a hypersaline-adapted
788 archaeon. BMC Genomics 13:351–351.

789 27. Gelsinger DR, DiRuggiero, J. 2018. Transcriptional landscape and regulatory roles of small
790 noncoding RNAs in the oxidative stress response of the haloarchaeon *Haloferax volcanii*. J
791 Bacteriol 200: e00779-17.

792 28. Lease RA, Smith, D, McDonough, K, Belfort, M. 2004. The small noncoding DsrA RNA is an
793 acid resistance regulator in *Escherichia coli*. J Bacteriol 186:6179–6185.

794 29. Majdalani N, Chen, S, Murrow, J, St John, K, Gottesman, S. 2001. Regulation of RpoS by a
795 novel small RNA: The characterization of RprA. Mol Microbiol 39:1382–1394.

796 30. Massé E, Gottesman, S. 2002. A small RNA regulates the expression of genes involved in
797 iron metabolism in *Escherichia coli*. Proc Natl Acad Sci U S A 99:4620–4625.

798 31. Delihas N, Forst, S. 2001. MicF: An antisense RNA gene involved in response of *Escherichia*
799 *coli* to global stress factors. J Mol Biol 313:1–12.

800 32. Lalaouna D, Baude, J, Wu, Z, Tomasini, A, Chicher, J, Marzi, S, Vandenesch, F, Romby, P,
801 Caldelari, I, Moreau, K. 2019. RsaC sRNA modulates the oxidative stress response of
802 *Staphylococcus aureus* during manganese starvation. Nucleic Acids Res 47:9871–9887.

803 33. Altuvia S, Weinstein-Fischer, D, Zhang, A, Postow, L, Storz, G. 1997. A small, stable RNA
804 induced by oxidative stress: Role as a pleiotropic regulator and antimutator. Cell 90:43–53.

805 34. Chen Y, Xue, D, Sun, W, Han, J, Li, J, Gao, R, Zhou, Z, Zhang, W, Chen, M, Lin, M, Wang, J,
806 Zuo, K. 2019. sRNA OsiA stabilizes catalase mRNA during oxidative stress response of
807 *Deincoccus radiodurans* R1. Microorganisms 7:422.

808 35. Gelsinger DR, Reddy, R, Whittington, K, Debic, S, DiRuggiero, J. 2021. Post-transcriptional
809 regulation of redox homeostasis by the small RNA SHOxi in haloarchaea. RNA Biol 18:1867–
810 1881.

811 36. Dantuluri S, Wu, Y, Hepowit, NL, Chen, H, Chen, S, Maupin-Furlow, JA. 2016. Proteome
812 targets of ubiquitin-like samp1ylation are associated with sulfur metabolism and oxidative
813 stress in *Haloferax volcanii*. Proteomics 16:1100–1110.

814 37. Halbeisen RE, Gerber, AP. 2009. Stress-dependent coordination of transcriptome and
815 translatome in yeast. PLOS Biol 7:e1000105.

816 38. Picard F, Loubière, P, Girbal, L, Cocaign-Bousquet, M. 2013. The significance of translation
817 regulation in the stress response. BMC Genomics 14:588.

818 39. Kuhn KM, DeRisi, JL, Brown, PO, Sarnow, P. 2001. Global and specific translational
819 regulation in the genomic response of *Saccharomyces cerevisiae* to a rapid transfer from a
820 fermentable to a nonfermentable carbon source. Mol Cell Biol 21:916–927.

821 40. Melamed D, Pnueli, L, Arava, Y. 2008. Yeast translational response to high salinity: Global
822 analysis reveals regulation at multiple levels. RNA 14:1337–1351.

823 41. Gerashchenko MV, Lobanov, AV, Gladyshev, VN. 2012. Genome-wide ribosome profiling
824 reveals complex translational regulation in response to oxidative stress. Proc Natl Acad Sci U S
825 A 109:17394–17399.

826 42. Benelli D, Marzi, S, Mancone, C, Alonzi, T, la Teana, A, Londei, P. 2008. Function and
827 ribosomal localization of aIF6, a translational regulator shared by archaea and eukarya.
828 Nucleic Acids Res 37:256–267.

829 43. Jäger D, Pernitzsch, SR, Richter, AS, Backofen, R, Sharma, CM, Schmitz, RA. 2012. An
830 archaeal sRNA targeting cis - and trans -encoded mRNAs via two distinct domains. Nucleic
831 Acids Res 40:10964–10979.

832 44. Prasse D, Ehlers, C, Backofen, R, Schmitz, RA. 2013. Regulatory RNAs in archaea: First target
833 identification in methanoarchaea. Biochem Soc Trans 41:344–349.

834 45. Altuvia S, Zhang, A, Argaman, L, Tiwari, A, Storz, G. 1998. The *Escherichia coli* OxyS
835 regulatory RNA represses *fhlA* translation by blocking ribosome binding. Embo J 17:6069–
836 6075; 6075.

837 46. Jevtić Ž, Stoll, B, Pfeiffer, F, Sharma, K, Urlaub, H, Marchfelder, A, Lenz, C. 2019. The
838 response of *Haloferax volcanii* to salt and temperature stress: A proteome study by label-free
839 mass spectrometry. Proteomics 19:1800491.

840 47. McMillan LJ, Hwang, S, Farah, RE, Koh, J, Chen, S, Maupin-Furlow, JA. 2018. Multiplex
841 quantitative SILAC for analysis of archaeal proteomes: A case study of oxidative stress
842 responses. Environ Microbiol 20:385–401.

843 48. Soborowski AL, Hackley, RK, Hwang, S, Zhou, G, Dulmage, K, Schönheit, P, Daniels, C, Bisson-
844 Filho, AW, Marchfelder, A, Maupin-Furlow, JA, Allers, T, Schmid, AK. 2024. Genomic re-
845 sequencing reveals mutational divergence across genetically engineered strains of model
846 archaea. bioRxiv 2024.08.08.607208.

847 49. Hawkins M, Malla, S, Blythe, MJ, Nieduszynski, CA, Allers, T. 2013. Accelerated growth in the
848 absence of DNA replication origins. Nature 503:544–547.

849 50. Hartman AL, Norais, C, Badger, JH, Delmas, S, Haldenby, S, Madupu, R, Robinson, J, Khouri,
850 H, Ren, Q, Lowe, TM, Maupin-Furlow, J, Pohlschroder, M, Daniels, C, Pfeiffer, F, Allers, T,
851 Eisen, JA. 2010. The complete genome sequence of *Haloferax volcanii* DS2, a model archaeon.
852 PLoS One 5:e9605.

853 51. Pohlschroder M, Schulze, S. 2019. *Haloferax volcanii*. Trends Microbiol 27:86–87.

854 52. Pérez-Arnaiz P, Dattani, A, Smith, V, Allers, T. 2020. *Haloferax volcanii*-a model archaeon for
855 studying DNA replication and repair. Open Biol 10:200293.

856 53. Gelsinger DR, Dallon, E, Reddy, R, Mohammad, F, Buskirk, AR, DiRuggiero, J. 2020. Ribosome
857 profiling in archaea reveals leaderless translation, novel translational initiation sites, and
858 ribosome pausing at single codon resolution. Nucleic Acids Res 48:5201–5216.

859 54. Hadjeras L, Bartel, J, Maier, L, Maaß, S, Vogel, V, Svensson, SL, Eggenhofer, F, Gelhausen, R,
860 Müller, T, Alkhnbashi, OS, Backofen, R, Becher, D, Sharma, CM, Marchfelder, A. 2023.
861 Revealing the small proteome of *Haloferax volcanii* by combining ribosome profiling and
862 small-protein optimized mass spectrometry. Microlife 4:uqad001.

863 55. Ingolia I, Ghaemmaghami, G, Newman, N, Weissman, W. 2009. Genome-wide analysis *in*
864 *vivo* of translation with nucleotide resolution using ribosome profiling. Science 324:218–223.

865 56. Gelsinger DR, DiRuggiero, J. 2018. Transcriptional landscape and regulatory roles of small
866 noncoding RNAs in the oxidative stress response of the haloarchaeon *Haloferax volcanii*. J
867 Bacteriol 200:e00779–17.

868 57. Pop C, Rouskin, S, Ingolia, NT, Han, L, Phizicky, EM, Weissman, JS, Koller, D. 2014. Causal
869 signals between codon bias, mRNA structure, and the efficiency of translation and elongation.
870 Mol Syst Biol 10:770.

871 58. Rak R, Dahan, O, Pilpel, Y. 2018. Repertoires of tRNAs: The couplers of genomics and
872 proteomics. Annu Rev Cell Dev Biol 34:239–264.

873 59. Babski J, Haas, KA, Näther-Schindler, D, Pfeiffer, F, Förstner, KU, Hammelmann, M, Hilker, R,
874 Becker, A, Sharma, CM, Marchfelder, A, Soppa, Jö. 2016. Genome-wide identification of
875 transcriptional start sites in the haloarchaeon *Haloferax volcanii* based on differential RNA-
876 seq (dRNA-seq). BMC Genomics 17:629.

877 60. Mi H, Muruganujan, A, Casagrande, JT, Thomas, PD. 2013. Large-scale gene function
878 analysis with the PANTHER classification system. Nat Protoc 8:1551–1566.

879 61. Mi H, Muruganujan, A, Huang, X, Ebert, D, Mills, C, Guo, X, Thomas, PD. 2019. Protocol
880 update for large-scale genome and gene function analysis with the PANTHER classification
881 system (v.14.0). Nat Protoc 14:703–721.

882 62. Szklarczyk D, Kirsch, R, Koutrouli, M, Nastou, K, Mehryary, F, Hachilif, R, Gable, AL, Fang, T,
883 Doncheva, NT, Pyysalo, S, Bork, P, Jensen, LJ, von Mering, C. 2023. The STRING database in
884 2023: Protein-protein association networks and functional enrichment analyses for any
885 sequenced genome of interest. Nucleic Acids Res 51:D638–D646.

886 63. Fine A, Irihimovitch, V, Dahan, I, Konrad, Z, Eichler, J. 2006. Cloning, expression, and
887 purification of functional Sec11a and Sec11b, type I signal peptidases of the archaeon
888 *Haloferax volcanii*. J Bacteriol 188:1911–1919.

889 64. Eichler J, Maupin-Furlow, J. 2013. Post-translation modification in archaea: Lessons from
890 *Haloferax volcanii* and other haloarchaea. FEMS Microbiol Rev 37:583–606.

891 65. Brooks CL, Lemieux, MJ. 2013. Untangling structure-function relationships in the rhomboid
892 family of intramembrane proteases. Biochim Biophys Acta 1828:2862–2872.

893 66. Urban S, Dickey, SW. 2011. The rhomboid protease family: A decade of progress on function
894 and mechanism. Genome Biol 12:231–231.

895 67. Parente J, Casabuono, A, Ferrari, MC, Paggi, RA, De Castro, RE, Couto, AS, Giménez, MI.
896 2014. A rhomboid protease gene deletion affects a novel oligosaccharide N-linked to the S-
897 layer glycoprotein of *Haloferax volcanii*. J Biol Chem 289:11304–11317.

898 68. De Castro RE, Giménez, MI, Cerletti, M, Paggi, RA, Costa, MI. 2022. Proteolysis at the
899 archaeal membrane: Advances on the biological function and natural targets of membrane-
900 localized proteases in *Haloferax volcanii*. Front Microbiol 13:940865.

901 69. Mondragon P, Hwang, S, Kasirajan, L, Oyetoro, R, Nasthas, A, Winters, E, Couto-Rodriguez,
902 RL, Schmid, A, Maupin-Furlow, JA. 2022. TrmB family transcription factor as a thiol-based
903 regulator of oxidative stress response. mBio 13:e0063322–22.

904 70. Llorca MG, Martínez-Espinosa, RM. 2022. Assessment of *Haloferax mediterranei* genome in
905 search of copper-molecular machinery with potential applications for bioremediation. Front
906 Microbiol 13:895296.

907 71. Liao Y, Williams, TJ, Ye, J, Charlesworth, J, Burns, BP, Poljak, A, Raftery, MJ, Cavicchioli, R.
908 2016. Morphological and proteomic analysis of biofilms from the antarctic archaeon,
909 *Halorubrum lacusprofundi*. Sci Rep 6:37454.

910 72. Reindel S, Anemüller, S, Sawaryn, A, Matzanke, BF. 2002. The DpsA-homologue of the
911 archaeon *Halobacterium salinarum* is a ferritin. Biochim Biophys Acta 1598:140–146.

912 73. Zeth K, Offermann, S, Essen, L, Oesterhelt, D. 2004. Iron-oxo clusters biomineralizing on
913 protein surfaces: Structural analysis of *Halobacterium salinarum* DpsA in its low- and high-iron
914 states. Proc Natl Acad Sci U S A 101:13780–13785.

915 74. Schulze S, Adams, Z, Cerletti, M, De Castro, R, Ferreira-Cerca, S, Fufezan, C, Giménez, MI,
916 Hippler, M, Jevtic, Z, Knüppel, R, Legerme, G, Lenz, C, Marchfelder, A, Maupin-Furlow, J, Paggi,
917 RA, Pfeiffer, F, Poetsch, A, Urlaub, H, Pohlschroder, M. 2020. The archaeal proteome project
918 advances knowledge about archaeal cell biology through comprehensive proteomics. Nat
919 Commun 11:3145.

920 75. Ndah E, Jonckheere, V, Giess, A, Valen, E, Menschaert, G, Van Damme, P. 2017.
921 REPARATION: Ribosome profiling assisted (re-)annotation of bacterial genomes. Nucleic Acids
922 Res 45:e168.

923 76. Sayers EW, Barrett, T, Benson, DA, Bolton, E, Bryant, SH, Canese, K, Chetvernin, V, Church,
924 DM, DiCuccio, M, Federhen, S, Feolo, M, Fingerman, IM, Geer, LY, Helmberg, W, Kapustin, Y,
925 Landsman, D, Lipman, DJ, Lu, Z, Madden, TL, Madej, T, Maglott, DR, Marchler-Bauer, A, Miller,
926 V, Mizrachi, I, Ostell, J, Panchenko, A, Phan, L, Pruitt, KD, Schuler, GD, Sequeira, E, Sherry, ST,
927 Shumway, M, Sirotkin, K, Slotta, D, Souvorov, A, Starchenko, G, Tatusova, TA, Wagner, L,
928 Wang, Y, Wilbur, WJ, Yaschenko, E, Ye, J. 2011. Database resources of the national center for
929 biotechnology information. Nucleic Acids Res 39:38.

930 77. Chen Y, Cao, X, Loh, KH, Slavoff, SA. 2023. Chemical labeling and proteomics for
931 characterization of unannotated small and alternative open reading frame-encoded
932 polypeptides. Biochem Soc Trans 51:1071–1082.

933 78. Will S, Joshi, T, Hofacker, IL, Stadler, PF, Backofen, R. 2012. LocARNA-P: Accurate boundary
934 prediction and improved detection of structural RNAs. RNA 18:900–914.

935 79. Wright PR, Georg, J, Mann, M, Sorescu, DA, Richter, AS, Lott, S, Kleinkauf, R, Hess, WR,
936 Backofen, R. 2014. CopraRNA and IntaRNA: Predicting small RNA targets, networks and
937 interaction domains. Nucleic Acids Res 42:119.

938 80. Thorsten A, Ngo Hien-Ping, Moshe, M, Lloyd Robert, G. 2004. Development of additional
939 selectable markers for the halophilic archaeon *Haloferax volcanii* based on the *leuB* and *trpA*
940 genes. Appl Environ Microbiol 70:943–953.

941 81. Rawls Katherine S., Martin Jonathan H., Maupin-Furlow Julie A. 2011. Activity and
942 transcriptional regulation of bacterial protein-like glycerol-3-phosphate dehydrogenase of the
943 haloarchaea in *Haloferax volcanii*. J Bacteriol 193:4469–4476.

944 82. Wang X, Liu, Q, Zhang, B. 2014. Leveraging the complementary nature of RNA-seq and
945 shotgun proteomics data. Proteomics 14:2676–2687.

946 83. de Sousa Abreu R, Penalva, LO, Marcotte, EM, Vogel, C. 2009. Global signatures of protein
947 and mRNA expression levels. Mol Biosyst 5:1512–1526.

948 84. Bąkowska-Żywicka K, Kasprzyk, M, Twardowski, T. 2016. tRNA-derived short RNAs bind to
949 *Saccharomyces cerevisiae* ribosomes in a stress-dependent manner and inhibit protein
950 synthesis in vitro. FEMS Yeast Res 16:fow077.

951 85. Holcik M, Sonenberg, N. 2005. Translational control in stress and apoptosis. Nat Rev Mol
952 Cell Biol 6:318–327.

953 86. Ivanov P, Kedersha, N, Anderson, P. 2019. Stress granules and processing bodies in
954 translational control. Cold Spring Harb Perspect Biol 11:a032813.

955 87. Hofmann S, Cherkasova, V, Bankhead, P, Bukau, B, Stoecklin, G. 2012. Translation
956 suppression promotes stress granule formation and cell survival in response to cold shock.
957 Mol Biol Cell 23:3786–3800.

958 88. Al-Fageeh MB, Smales, CM. 2009. Cold-inducible RNA binding protein (CIRP) expression is
959 modulated by alternative mRNAs. RNA 15:1164–1176.

960 89. Costa ED, Chai, Y, Winans, SC. 2012. The quorum-sensing protein TraR of *Agrobacterium*
961 *tumefaciens* is susceptible to intrinsic and TraM-mediated proteolytic instability. Mol
962 Microbiol 84:807–815.

963 90. Dessaux Y, Faure, D. 2018. Quorum sensing and quorum quenching in *Agrobacterium*: A
964 "go/no go system"? Genes (Basel) 9:210.

965 91. Turnbough CLJ. 2019. Regulation of bacterial gene expression by transcription attenuation.
966 Microbiol Mol Biol Rev 83:e00019–19.

967 92. Xiu Z, Chang, Z, Zeng, A. 2002. Nonlinear dynamics of regulation of bacterial trp operon:
968 Model analysis of integrated effects of repression, feedback inhibition, and attenuation.
969 Biotechnol Prog 18:686–693.

970 93. Aoyama JJ, Raina, M, Zhong, A, Storz, G. 2022. Dual-function spot 42 RNA encodes a 15–
971 amino acid protein that regulates the CRP transcription factor. Proc Natl Acad Sci U S A
972 119:e2119866119.

973 94. Raina M, King, A, Bianco, C, Vanderpool, CK. 2018. Dual-function RNAs. Microbiol Spectr
974 6:10.1128/microbiolspec.rwr–2018.

975 95. Lloyd CR, Park, S, Fei, J, Vanderpool, CK. 2017. The small protein SgrT controls transport
976 activity of the glucose-specific phosphotransferase system. J Bacteriol 199:e00869–16.

977 96. Tufail MA, Jordan, B, Hadjeras, L, Gelhausen, R, Cassidy, L, Habenicht, T, Gutt, M, Hellwig, L,
978 Backofen, R, Tholey, A, Sharma, CM, Schmitz, RA. 2024. Uncovering the small proteome of
979 *Methanosarcina mazei* using ribo-seq and peptidomics under different nitrogen conditions.
980 Nat Commun 15:8659.

981 97. Raina M, Aoyama, JJ, Bhatt, S, Paul, BJ, Zhang, A, Updegrove, TB, Miranda-Ríos, J, Storz, G.
982 2022. Dual-function AzuCR RNA modulates carbon metabolism. Proc Natl Acad Sci U S A
983 119:e2117930119.

984 98. Guttman M, Russell, P, Ingolia, NT, Weissman, JS, Lander, ES. 2013. Ribosome profiling
985 provides evidence that large noncoding RNAs do not encode proteins. Cell 154:240–251.

986 99. Gelhausen R, Müller, T, Svensson, SL, Alkhnbashi, OS, Sharma, CM, Eggenhofer, F, Backofen,
987 R. 2022. RiboReport - benchmarking tools for ribosome profiling-based identification of open
988 reading frames in bacteria. Brief Bioinform 23:bbab549.

989 100. Gebetsberger J, Zywicki, M, Künzi, A, Polacek, N. 2012. tRNA-derived fragments target the
990 ribosome and function as regulatory non-coding RNA in *Haloferax volcanii*. Archaea
991 2012:260909.

992 101. Wyss L, Waser, M, Gebetsberger, J, Zywicki, M, Polacek, N. 2018. mRNA-specific
993 translation regulation by a ribosome-associated ncRNA in *Haloferax volcanii*. Sci Rep 8:12502.

994 102. Collins JA, Irnov, I, Baker, S, Winkler, WC. 2007. Mechanism of mRNA destabilization by the
995 *glmS* ribozyme. Genes Dev 21:3356–3368.

996 103. Desnoyers G, Morissette, A, Prévost, K, Massé, E. 2009. Small RNA-induced differential
997 degradation of the polycistronic mRNA iscRSUA. Embo J 28:1551–1561.

998 104. Märtens B, Manoharadas, S, Hasenöhrl, D, Manica, A, Bläsi, U. 2013. Antisense regulation
999 by transposon-derived RNAs in the hyperthermophilic archaeon *Sulfolobus solfataricus*.
1000 EMBO Rep 14:527–533.

1001 105. Bernick DL, Dennis, PP, Höchsmann, M, Lowe, TM. 2012. Discovery of *Pyrobaculum* small
1002 RNA families with atypical pseudouridine guide RNA features. RNA 18:402–411.

1003 106. Goldberger O, Livny, J, Bhattacharyya, R, Amster-Choder, O. 2021. Wisdom of the crowds:
1004 A suggested polygenic plan for small-RNA-mediated regulation in bacteria. iScience
1005 24:103096.

1006 107. Westermann AJ. 2018. Regulatory RNAs in virulence and host-microbe interactions.
1007 Regulating with RNA in Bacteria and Archaea 6:305–337.

1008 108. Gelsinger, DR, Dallon, E, DiRuggiero, J. 2022. Conversion of Ribosome-Protected mRNA to
1009 DNA and Deep Sequencing for Ribosome Profiling in *Haloferax volcanii*, p. 223–242. *In* S.
1010 Ferreira-Cerca (ed.), Archaea: Methods and Protocols. Springer US, New York, NY.
1011 https://doi.org/10.1007/978-1-0716-2445-6_14.

1012 109. Martin M. 2011. Cutadapt removes adapter sequences from high-throughput sequencing
1013 reads. EMBnet.Journal 17:10-12.

1014 110. Langmead B, Trapnell, C, Pop, M, Salzberg, SL. 2009. Ultrafast and memory-efficient
1015 alignment of short DNA sequences to the human genome. Genome Biol 10:R25.

1016 111. Li H, Handsaker, B, Wysoker, A, Fennell, T, Ruan, J, Homer, N, Marth, G, Abecasis, G,
1017 Durbin, R, 1000 Genome Project Data Processing Subgroup. 2009. The sequence
1018 alignment/map format and SAMtools. Bioinformatics 25:2078–2079.

1019 112. Pertea M, Pertea, GM, Antonescu, CM, Chang, T, Mendell, JT, Salzberg, SL. 2015. StringTie
1020 enables improved reconstruction of a transcriptome from RNA-seq reads. Nat Biotechnol
1021 33:290–295.

1022 113. Liao Y, Smyth, GK, Shi, W. 2014. featureCounts: An efficient general purpose program for
1023 assigning sequence reads to genomic features. Bioinformatics 30:923–930.

1024 114. Love MI, Huber, W, Anders, S. 2014. Moderated estimation of fold change and dispersion
1025 for RNA-seq data with DESeq2. Genome Biol 15:550.

1026 115. Thomas PD, Ebert, D, Muruganujan, A, Mushayahama, T, Albou, L, Mi, H. 2022. PANTHER:
1027 Making genome-scale phylogenetics accessible to all. Protein Sci 31:8–22.

1028 116. Moran HM, Manriquez-Sandoval, E, Sharma, P, Fried, SD, Gillilan, RE. 2024. Proteome-wide
1029 assessment of protein structural perturbations under high pressure. PRX Life 2:033011.

1030 117. To P, Whitehead, B, Tarbox, HE, Fried, SD. 2021. Nonrefoldability is pervasive across the *E.*
1031 *coli* proteome. J Am Chem Soc 143:11435–11448.

1032 118. Dyall-Smith, M. 2009. The Halohandbook – Protocols for haloarchaeal genetics. Available
1033 at https://haloarchaea.com/wp-content/uploads/2025/02/Halohandbook_2009_REV_v2.pdf.

1034 119. Fu X, Adams, Z, Maupin-Furlow, J. 2019. Assays for ubiquitin-like protein ligation and
1035 proteasome function in archaea. Methods Enzymol 619:161–178.

1036 120. Altschul SF, Gish, W, Miller, W, Myers, EW, Lipman, DJ. 1990. Basic local alignment search
1037 tool. J Mol Biol 215:403–410.

1038 121. Mann M, Wright, PR, Backofen, R. 2017. IntaRNA 2.0: Enhanced and customizable
1039 prediction of RNA–RNA interactions. Nucleic Acids Res 45:W435–W439.

1040 122. Livak KJ, Schmittgen, TD. 2001. Analysis of relative gene expression data using real-time
1041 quantitative PCR and the 2(-delta delta C(T)) method. Methods 25:402–408.

1042 123. Perez-Riverol Y, Bandla, C, Kundu, DJ, Kamatchinathan, S, Bai, J, Hewapathirana, S, John,
1043 NS, Prakash, A, Walzer, M, Wang, S, Vizcaíno, JA. 2024. The PRIDE database at 20 years: 2025
1044 update. Nucleic Acids Res 53:D543–D553.

1045

Figures

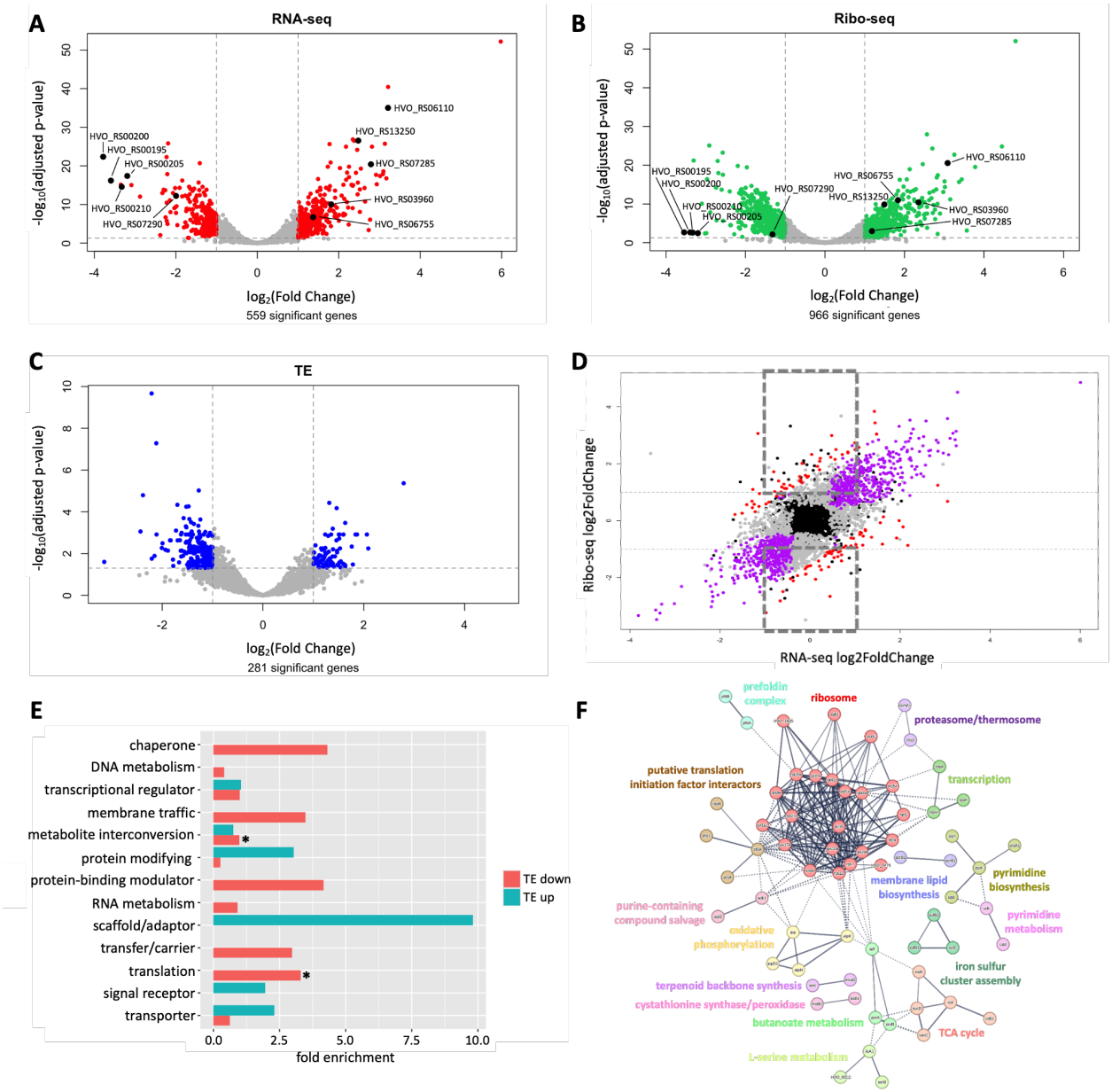

Figure 1. Comparison of genes with differential transcription, ribosome occupancy, and translation during oxidative stress. Volcano plots of $\log_2$ fold changes and corresponding $-\log_{10}$ p-values of transcript abundances (A), ribosome occupancies (B), and TE (C) comparing stress vs no stress conditions. Red, green, and blue colored points highlight transcripts with differential expression (adjusted p-value <0.05 and absolute $\log_2$ fold change >1). Fold change and p-values were calculated using DESeq2. Labeled black points indicate genes previously shown to be involved in oxidative stress response. All other genes are shown in gray. D. Scatterplot comparing $\log_2$ fold change for transcript abundances and ribosome occupancies. Genes with significant p-value (<0.05) in RNA-seq or Ribo-seq data are shown in gray, while those with a significant p-value in both are shown in purple. Genes with differential TE are shown in red. All

other genes (non-significant) are shown in black. Dark gray boxes encompass genes that are predicted to change at the translation level only. E. Functional categories (protein class) of genes with differential TE during oxidative stress. Functions of significant genes were categorized using PANTHER generic mapping based on homology. Enrichment was calculated for genes in each category using the total number of PANTHER hits (2061 for the full proteome, 99 for TE down, and 42 for TE up). Asterisks indicate significant categories (translation) or categories that contain significantly enriched subcategories (ribosomal proteins; peroxidases). F. STRING network depicting predicted interactions for genes with downregulated TE during oxidative stress. Nodes depict individual genes, with predicted interaction as edges. Edge thickness indicates increasing interaction confidence, where thinner edges have a confidence score of at least 0.7 and thicker edges have a confidence score of at least 0.9. Dotted lines indicate edges between clusters. Genes with no predicted interactions are not shown. Node color indicates functional clusters.

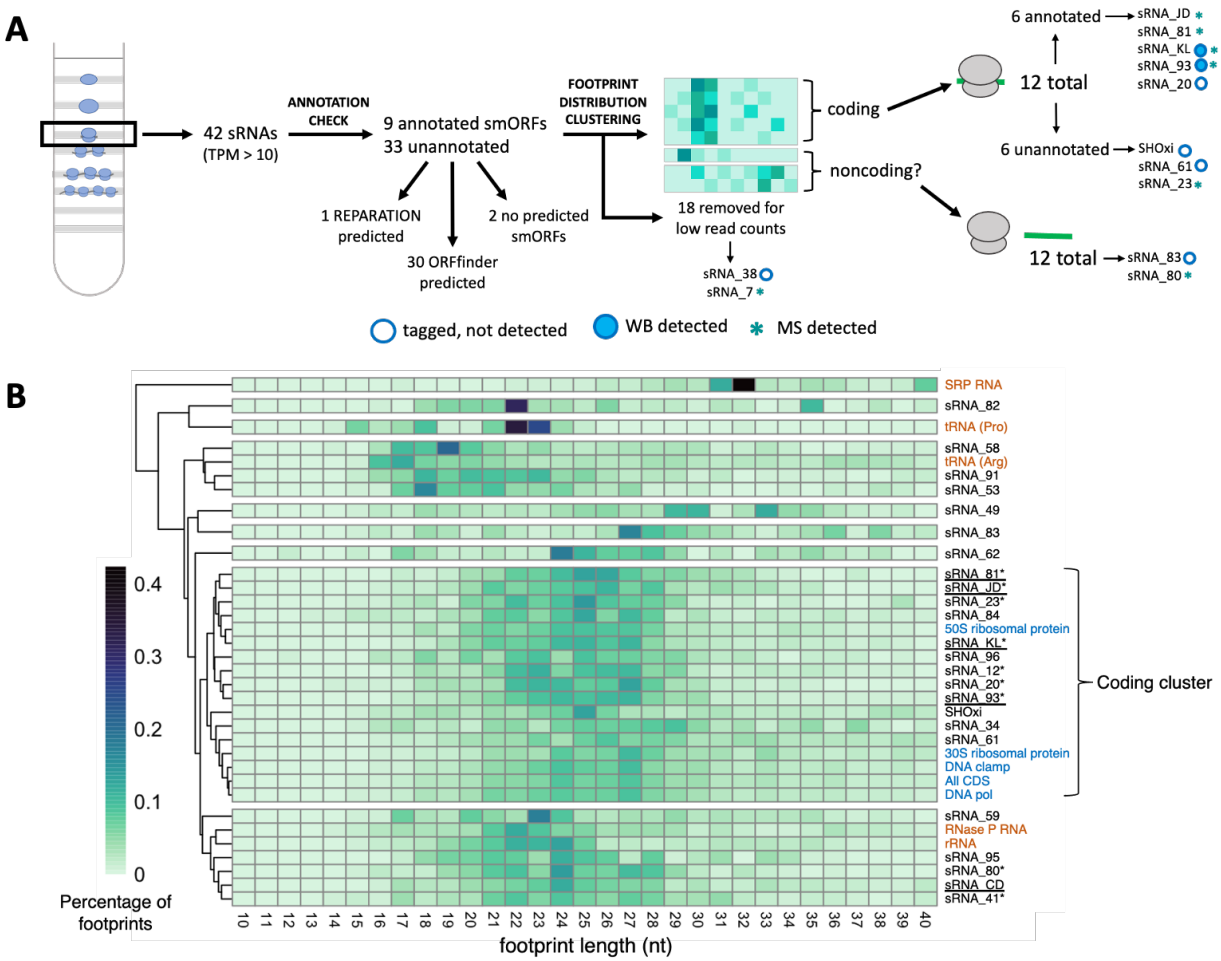

Figure 2. Ribosome footprint length distributions and sRNAs with ribosome occupancy. A. Schematic of analyses to assess the coding potential for sRNAs with ribosome occupancy, starting with the isolation of monosome fractions during ribosome profiling. B. Clustered heatmap of ribosome footprint length distributions for sRNAs, coding genes, and noncoding genes with ribosome occupancy under control conditions. Darker colors indicate higher read percentage. Known coding genes are shown in blue, known noncoding genes in orange, and sRNAs in black. sRNAs with annotated proteins are underlined. sRNAs for which peptides have been detected by MS are marked with an asterisk.

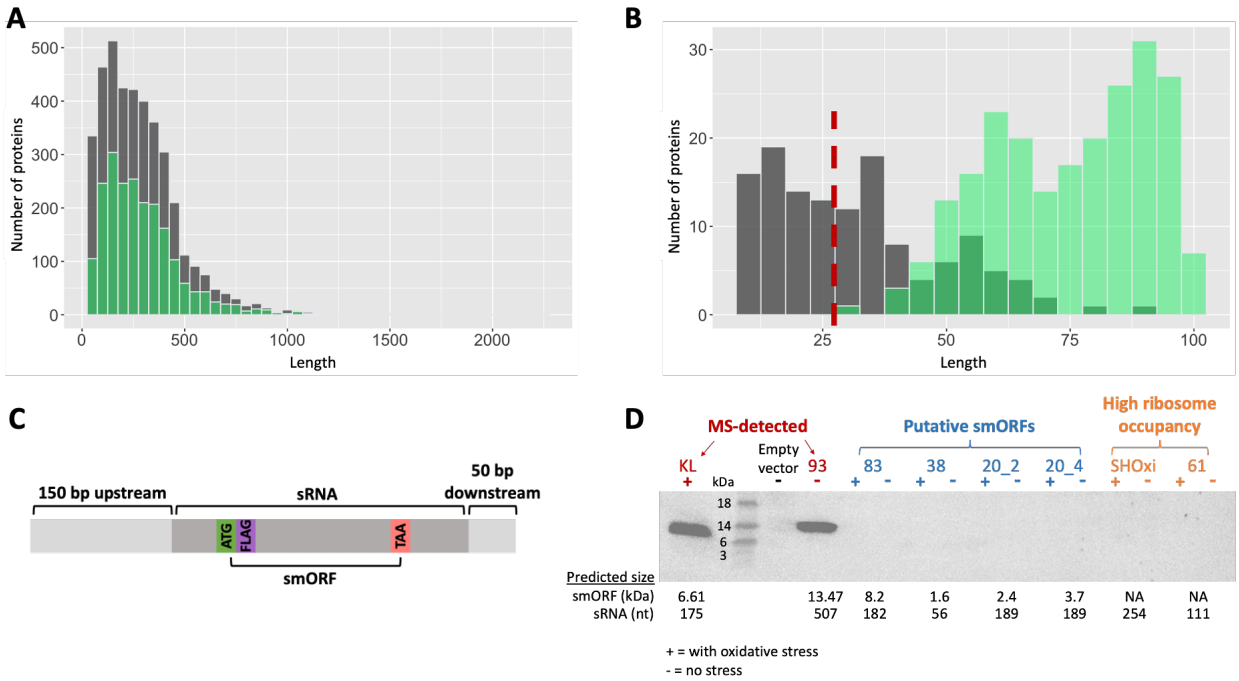

Figure 3. Discovery of novel small proteins encoded in sRNAs. A. Histogram of protein length (aa) for the *H. volcanii* annotated proteome (gray) and proteins detected by MS (green). B. Histogram of protein length (aa) for putative peptides (predicted using NCBI ORF finder) encoded by sRNAs (gray) and small proteins detected by MS (green). Detection cutoff of 30aa is indicated by red dashed line. C. Cloning strategy for tagging sRNAs for Western blot analysis. FLAG indicates the location of the 3xFLAG-tag. D. Western blot of tagged sRNAs. + indicates samples treated with hydrogen peroxide and - indicates control samples.

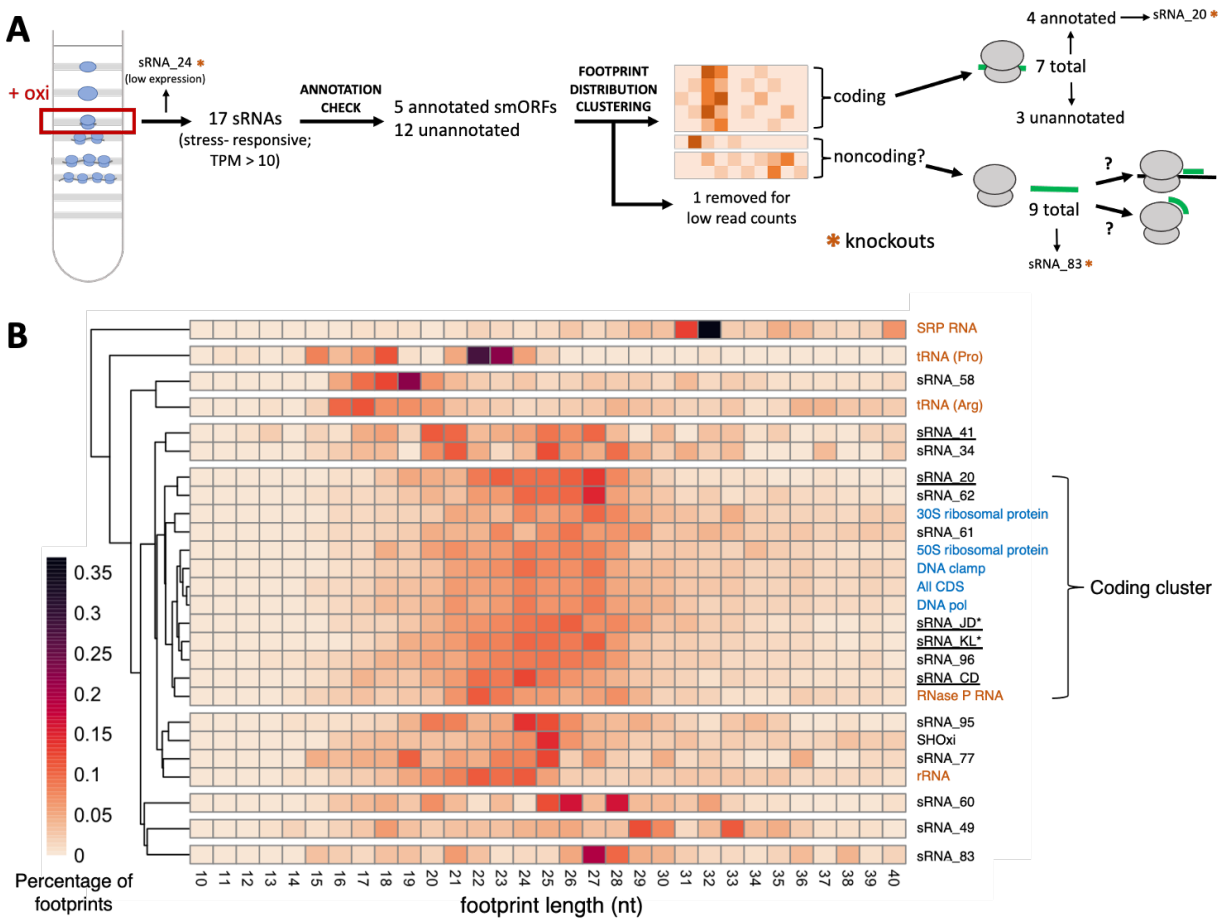

Figure 4. Ribosome footprint length distributions and stress-responsive sRNAs with ribosome occupancy. A. Schematic of analyses to assess the coding potential for sRNAs with ribosome occupancy, starting with the isolation of monosome fractions on a sucrose gradient using samples treated with oxidative stress. B. Clustered heatmaps of ribosome footprint length distributions for sRNAs, coding genes, and noncoding genes with ribosome occupancy under oxidative stress. Darker colors indicate higher read percentage. Known coding genes are shown in blue, known noncoding genes in orange, and sRNAs in black. sRNAs with annotated proteins are underlined. sRNAs for which peptides have been detected by MS are marked with an asterisk.

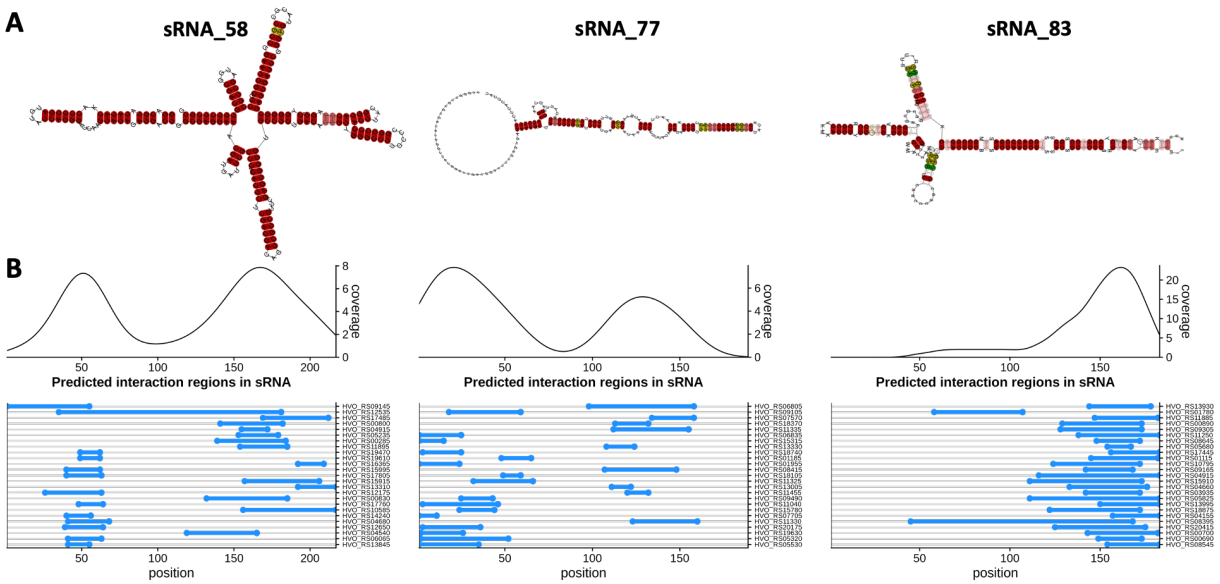

Figure 5. Characterization of stress-responsive sRNAs with ribosome occupancy. A. Consensus RNA structural predictions for sRNAs with no evidence of coding potential were generated using LocARNA. Colored bases indicate sequence and structural conservation of compatible base pairs within the predicted structure. Colors correspond to number of base pair types (red: 1, yellow: 2, green: 3) with red being the most highly conserved and green the least conserved. Color saturation decreases with the number of incompatible base pairs. B. IntaRNA was used to predict putative mRNA targets (Tables S13-15). Blue lines indicate putative binding regions along the sRNA. Curves depict coverage of putative binding regions along the sRNA.